A European aerosol phenomenology – 9: Light absorption properties of carbonaceous aerosol particles across surface Europe

Jordi Rovira, Marjan Savadkoohi, Gang Chen, Griša Močnik, Wenche Aas, Lucas Alados-Arboledas, Begoña Artiñano, Minna Aurela, John Backman, Sujai Banerji, et al.

Environment International 195 (2025) 109185

Contents lists available at ScienceDirect

Environment International

journal homepage: www.elsevier.com/locate/envint

Full length article

A European aerosol phenomenology – 9: Light absorption properties of carbonaceous aerosol particles across surface Europe

Jordi Rovira [a,b,*], Marjan Savadkoohi [a,c], Gang I. Chen [d], Griša Močnik [e,f,g], Wenche Aas [h], Lucas Alados-Arboledas [i], Begoña Artiñano [j], Minna Aurela [k,l], John Backman [k], Sujai Banerji [m], David Beddow [n], Benjamin Brem [o], Benjamin Chazeau [o,p], Martine Collaud Coen [q], Cristina Colombi [r], Sebastien Conil [s], Francesca Costabile [t], Esther Coz [i], Joel F. de Brito [u], Kostas Eleftheriadis [v], Olivier Favez [w], Harald Flentje [x], Evelyn Freney [y], Asta Gregorič [e,z], Martin Gysel-Beer [o], Roy Harrison [m,aa], Christoph Hueglin [ab], Antti Hyvärinen [k], Matic Ivančič [z], Athina-Cerise Kalogridis [v], Hannes Keernik [ac], Granakis Konstantinos [v], Paolo Laj [l,ad], Eleni Liakakou [ae], Chunshui Lin [af], Stefano Listrani [ag], Krista Luoma [k,m], Marek Maasikmets [ac], Hanna E. Manninen [ah], Nicolas Marchand [p], Sebastiao Martins dos Santos [ai], Saliou Mbengue [aj], Nikos Mihalopoulos [ae], Doina Nicolae [ak], Jarkko V. Niemi [ah], Michael Norman [al], Jurgita Ovadnevaite [af], Jean-Eudes Petit [am], Stephen Platt [h], André S.H. Prévôt [o], Manuel Pujadas [j], Jean-Philippe Putaud [ai], Véronique Riffault [u], Martin Rigler [z], Matteo Rinaldi [an], Jaroslav Schwarz [ao], Sanna Silvergren [al], Erik Teinemaa [ac], Kimmo Teinilä [k], Hilkka Timonen [k], Gloria Titos [i], Anna Tobler [o,ap], Jeni Vasilescu [ak], Stergios Vratolis [v], Karl Espen Yttri [h], Eduardo Yubero [aq], Naděžda Zíková [ao], Andrés Alastuey [a], Tuukka Petäjä [m], Xavier Querol [a], Jesús Yus-Díez [e], Marco Pandolfi [a,*]

[a] Institute of Environmental Assessment and Water Research (IDAEA-CSIC), 08034 Barcelona, Spain
[b] Department of Applied Physics-Meteorology, Universitat de Barcelona, Barcelona, 08028, Spain
[c] Department of Mining, Industrial and ICT Engineering (EMIT), Manresa School of Engineering (EPSEM), Universitat Politècnica de Catalunya (UPC), Manresa 08242, Spain
[d] Environmental Research Group, MRC Centre for Environment and Health, Imperial College London, London W12 0BZ, UK
[e] Center for Atmospheric Research, University of Nova Gorica, Ajdovščina 5270, Slovenia
[f] Haze Instruments d.o.o., Ljubljana 1000, Slovenia
[g] Department of Condensed Matter Physics, Jozef Stefan Institute, Ljubljana, 1000, Slovenia
[h] NILU, 2027 Kjeller, Norway
[i] Andalusian Institute for Earth System Research (IISTA-CEAMA), University of Granada, Granada, Spain
[j] Environment Department, CIEMAT, Madrid, Spain
[k] Atmospheric Composition Research, Finnish Meteorological Institute, 00560 Helsinki, Finland
[l] Aerosol Physics Laboratory, Faculty of Engineering and Natural Sciences, Tampere University, Tampere University, P.O. Box 692, FI-33014, Finland
[m] Institute for Atmospheric and Earth System Research/Physics (INAR), Faculty of Science, University of Helsinki, Helsinki, Finland
[n] Division of Environmental Health & Risk Management, School of Geography, Earth & Environmental Sciences, University of Birmingham, Edgbaston, Birmingham, UK
[o] PSI Center for Energy and Environmental Sciences, Paul Scherrer Institute, 5232 Villigen PSI, Switzerland
[p] Aix Marseille Univ., CNRS, LCE, Marseille, France
[q] Federal Office of Meteorology and Climatology, MeteoSwiss, Payerne, Switzerland
[r] Arpa Lombardia, Settore Monitoraggi Ambientali, Unità Operativa Qualità dell'Aria, Milano, Italy
[s] ANDRA DRD/GES Observatoire Pérenne de l'Environnement, 55290 Bure, France
[t] Institute of Atmospheric Sciences and Climate (ISAC), National Research Council (CNR), 00133, Rome, Italy
[u] IMT Nord Europe, Institut Mines-Télécom, Univ. Lille, Centre for Energy and Environment, Lille, France
[v] ENRACT, Institute of Nuclear and Radiological Science & Technology, Energy & Safety, NCSR Demokritos, 15310 Ag. Paraskevi, Athens, Greece

* Corresponding authors at: Institute of Environmental Assessment and Water Research (IDAEA-CSIC), 08034 Barcelona, Spain (Jordi Rovira).
E-mail addresses: jordi.rovira@idaea.csic.es (J. Rovira), marco.pandolfi@idaea.csic.es (M. Pandolfi).

https://doi.org/10.1016/j.envint.2024.109185
Received 2 September 2024; Received in revised form 7 November 2024; Accepted 4 December 2024
Available online 9 December 2024

[w] Institut National de l'Environnement Industriel et des Risques (INERIS), Verneuil-en-Halatte, France
[x] German Meteorological Service (DWD), Observatory Hohenpeissenberg, Germany
[y] Laboratoire de Météorologie Physique, UMR6016, Université Clermont Auvergne-CNRS, Aubière, France
[z] Aerosol d.o.o., Kamniška 39A, 1000 Ljubljana, Slovenia
[aa] Department of Environmental Sciences, Faculty of Meteorology, Environment and Arid Land Agriculture, King Abdulaziz University, Jeddah, Saudi Arabia
[ab] Laboratory for Air Pollution and Environmental Technology, Swiss Federal Laboratories for Materials Science and Technology (Empa), Duebendorf, Switzerland
[ac] Estonian Environmental Research Centre, Air Quality Management Department, Tallinn, Estonia
[ad] Univ. Grenoble, CNRS, IRD, IGE, 38000 Grenoble, France
[ae] Institute for Environmental Research & Sustainable Development, National Observatory of Athens, Athens, Greece
[af] School of Natural Sciences, Physics, Centre for Climate and Air Pollution Studies, Ryan Institute, University of Galway, University Road, Galway H91 CF50, Ireland
[ag] ARPA Lazio, Regional Environmental Protection Agency, Rome, Italy
[ah] Helsinki Region Environmental Services Authority (HSY), Helsinki, Finland
[ai] European Commission, Joint Research Centre (JRC), Ispra, Italy
[aj] Global Change Research Institute, Czech Academy of Sciences, 603 00 Brno, Czech Republic
[ak] National Institute of Research and Development for Optoelectronics INOE 2000, Magurele, Romania
[al] Environment and Health Administration, SLB-analysis, Stockholm, Sweden
[am] Laboratoire des Sciences du Climat et de l'Environnement, CEA/Orme des Merisiers, Gif-sur-Yvette, France
[an] Institute of Atmospheric Sciences and Climate (ISAC), National Research Council (CNR), 40129 Bologna, Italy
[ao] Institute of Chemical Process Fundamentals of the CAS, Rozvojová 135/1, 16502 Prague, Czech Republic
[ap] Datalystica Ltd., Parkstrasse 1, 5234 Villigen, Switzerland
[aq] Atmospheric Pollution Laboratory (LCA), Department of Applied Physics, Miguel Hernández University, Elche 03202, Spain

ARTICLE INFO

Handling Editor: Adrian Covaci

Keywords:
European overview
Organic aerosols
Long-term datasets
Light absorption
Air quality

ABSTRACT

Carbonaceous aerosols (CA), composed of black carbon (BC) and organic matter (OM), significantly impact the climate. Light absorption properties of CA, particularly of BC and brown carbon (BrC), are crucial due to their contribution to global and regional warming. We present the absorption properties of BC ($b_{Abs,BC}$) and BrC ($b_{Abs,BrC}$) inferred using Aethalometer data from 44 European sites covering different environments (traffic (TR), urban (UB), suburban (SUB), regional background (RB) and mountain (M)). Absorption coefficients showed a clear relationship with station setting decreasing as follows: TR > UB > SUB > RB > M, with exceptions. The contribution of $b_{Abs,BrC}$ to total absorption (b_{Abs}), i.e. $\%Abs_{BrC}$, was lower at traffic sites (11–20 %), exceeding 30 % at some SUB and RB sites. Low AAE values were observed at TR sites, due to the dominance of internal combustion emissions, and at some remote RB/M sites, likely due to the lack of proximity to BrC sources, insufficient secondary processes generating BrC or the effect of photobleaching during transport. Higher b_{Abs} and AAE were observed in Central/Eastern Europe compared to Western/Northern Europe, due to higher coal and biomass burning emissions in the east. Seasonal analysis showed increased b_{Abs}, $b_{Abs,BC}$, $b_{Abs,BrC}$ in winter, with stronger $\%Abs_{BrC}$, leading to higher AAE. Diel cycles of $b_{Abs,BC}$ peaked during morning and evening rush hours, whereas $b_{Abs,BrC}$, $\%Abs_{BrC}$, AAE, and AAE_{BrC} peaked at night when emissions from household activities accumulated. Decade-long trends analyses demonstrated a decrease in b_{Abs}, due to reduction of BC emissions, while $b_{Abs,BrC}$ and AAE increased, suggesting a shift in CA composition, with a relative increase in BrC over BC. This study provides a unique dataset to assess the BrC effects on climate and confirms that BrC can contribute significantly to UV–VIS radiation presenting highly variable absorption properties in Europe.

1. Introduction

Carbonaceous aerosols (CA), composed of organic matter(OM) and black carbon (BC), play a significant role in the climate system. CA particles can modify the radiative budget through direct absorption and scattering of solar radiation, through semi-direct effects by modifying the thermodynamic state of the surrounding atmosphere, and indirectly by altering the cloud formation processes. The latest Intergovernmental Panel on Climate Change report (IPCC, 2021) considers CA particles to be key short-lived climate pollutants and presents climate scenarios where mitigating their emissions, in particular of BC, can result in both climate and health co-benefits (e.g., Harmsen et al., 2020).

Black carbon, emitted as a product of the incomplete combustion of fossil fuels and biofuels, is the most effective aerosol warming agent given its ability to efficiently absorb radiation from the ultraviolet (UV) to the infrared (IR) part of the spectrum (Bond and Bergstrom, 2006; Bond et al., 2013; Lin et al., 2023). Until recently, BC was considered to be the second largest warming agent after CO_2 (e.g. IPCC, 2013; Samset et al. 2014; Samset et al. 2018) but the latest estimates suggest that the warming effect of BC emissions could be lower than originally thought (IPCC, 2021; Harmsen et al., 2020 and references herein), mostly due to the simultaneous interactions of warming BC and co-emitted cooling agents such as OM with the solar radiation. Organic particulate matter, in fact, constitutes a large fraction of the atmospheric aerosol mass (20–90 %; Jimenez et al., 2009) and is estimated to exert a net cooling effect on a global level (e.g., IPCC, 2021). However, there is an increasing number of observations demonstrating the light-absorbing properties of a significant fraction of OM, usually referred to as brown carbon (BrC; e.g. Kirchstetter et al., 2004; Saleh et al., 2018, 2020; Samset et al., 2018; Sumlin et al., 2018, Kumar et al., 2023 among others).

BrC particulate matter (BrC PM) is a complex collection of light-absorbing organic molecules that can be soluble in solvents (such as water, methanol, and acetone) or insoluble (e.g. Corbin et al., 2018 and references therein) and that can efficiently absorb light in the ultraviolet (UV) and shorter visible wavelengths (Kirchstetter et al, 2004; Samset et al., 2018; Laskin et al., 2015; Moise et al., 2015; Saleh et al., 2018, 2020). BrC PM has attracted much attention due to its potential impacts on the Earth's radiative budget (Feng et al., 2013; Chakrabarty et al., 2016), the atmospheric chemical processes it undergoes (Liu et al., 2016; Wong et al., 2017), and its potential effect on human health (Yan et al., 2018). However, the lack of a complete description of BrC light absorption properties impairs the accurate estimation of its effects on climate warming. Fossil fuels, biofuels and biomass burning have been identified as the most important sources of primary and secondary BrC at a global scale (Zhang et al., 2020; Qin et al., 2018; Yan et al., 2017; Feng et al., 2013; Chen et al., 2020). In particular, biomass burning emissions have been confirmed as one of the most important sources of BrC (Washenfelder et al., 2015; Zhang et al., 2020). Moreover, recent studies have shown the light-absorbing properties of other BrC sources

of anthropogenic origin such as vehicular emissions (Qin et al., 2018; Hu et al., 2017; Moschos et al., 2018; Zhang et al., 2020; Ho et al., 2023), human-engineered materials (Hopstock et al., 2023), marine diesel engine operated on heavy fuel oil (e.g. Corbin et al., 2018; Yang et al., 2024), and coal combustion (e.g. Ni et al., 2021), among others. The emissions from the aforementioned sources can produce secondary BrC either through production of absorbing organics or coating of BC (Kalbermatter et al., 2022), i.e. secondary organic aerosols (SOA) with varying absorptive properties (e.g. Kumar et al., 2018). Moreover, after emission or formation, BrC PM can undergo physico-chemical processes such as a reduction of BrC light absorption primarily related to photochemical processes called photobleaching (e.g. Fang et al., 2023) or may lead to substantial reduction of NO2 photolysis and drop in O3 concentrations (Laskin et al., 2015). Although OM has been historically considered as essentially non-absorbing particulate matter, there has been a shift over the past 10 years to include their absorptive properties in climate models (e.g. Feng et al., 2013, Saleh et al., 2020). Indeed, some studies have found BrC responsible for 20–50 % of the total aerosol light-absorption in the UV (e.g. Shamjad et al., 2016; Wang et al., 2016; Li et al., 2022), and that the inclusion of strongly absorbing BrC in global climate models causes a shift of the direct radiative forcing of OM at the top of the atmosphere from a net cooling to a warming effect (Feng et al., 2013; Wang et al., 2013). Notably, model estimations have shown that the atmospheric heating of BrC from wildfires in the tropical mid and upper troposphere is larger than that of BC (Zhang et al., 2020). However, due to the complex processes forming and modifying BrC PM, their large spatial and temporal variability, and the lack of an exhaustive characterization of their optical properties at ambient conditions, the contribution of BrC on climate is still under-represented in current models (Brown et al., 2018, Zhang et al., 2020; Sand et al., 2021). Moreover, the dearth of long-term observations of BrC optical properties also limits the possibility to efficiently constrain the modeled properties of BrC PM (e.g., Yan et al., 2018).

In the last decade several studies have reported the BrC contribution to absorption in different cities in Europe, with special interest on winter conditions and on the contribution from wood burning and heating systems. For example, the results reported in Ferrero et al. (2018, 2021) for Northern Italy, Moschos et al. (2021) for Switzerland, Zhang et al. (2020) and Velazquez-Garcia et al., (2023) for France, Liakakou et al. (2020) and Kaskaoutis et al. (2024) for Greece and López-Caravaca et al. (2024) for Spain showed that the BrC contribution to total aerosol absorption at 370 nm ranged between around 20 % and 40 %. Contributions as high as 60–70 % were observed in winter in Slovenia (Cuesta-Mosquera et al., 2024) and in areas with old wooden houses and outdated heating systems as reported by Pauraite et al. (2023) for Lithuania. Overall, these studies have shown the high spatial and seasonal variability of BrC contribution to total absorption across Europe, related to differences in BrC sources, atmospheric conditions, station background (i.e. urban vs. regional), geographical location (i.e. open plains vs. enclosed valleys) and altitude.

Besides the high variability of the BrC contribution to absorption across Europe, BrC PM represents a subset of organic particles species that also exhibit very different wavelength dependent absorption properties. This wavelength dependency is represented through the Absorption Ångström Exponent (AAE), a key parameter for assessing the radiative forcing and climate effects of atmospheric aerosol particles. The AAE allows the absorption measured at a given wavelength to be reported at any other wavelength within the spectral range where the AAE was determined. Moreover, the AAE is an intensive aerosol particle optical property, i.e., it describes relative spectral contribution of particles to absorption independently of the total particle concentration. The imaginary refractive index of BrC progressively increases from the visible toward the UV, therefore, causing the AAE of BrC PM (AAE_{BrC} from now on) to be higher than that of BC, which has approximately constant imaginary refractive index. In addition, the absorbing properties of BrC are quite variable which translates to considerable variability of AAE_{BrC} (e.g. Lack and Langridge, 2013; Kumar et al., 2023). Ambient measurements have confirmed the high variability of AAE_{BrC} and values ranging between around 3 and 9 were reported in literature (e.g. Srinivas and Sarin, 2013; Massabò et al., 2015; Ferrero et al., 2018; Cuesta-Mosquera et al., 2024). Moreover, a wide range of AAE values for BrC PM generated in chamber experiments was provided by Saleh et al. (2013, 2020). Saleh et al. (2013, 2020) reported the Ångström exponent of the imaginary refractive index k (called ω) which is related to AAE_{BrC} by a simple relationship in the small particle limit of $AAE_{BrC} = \omega + 1$. The ω presented by Saleh et al. (2013, 2020) ranged from values higher than 7 for secondary organic aerosols from aromatic VOCs to values around 2–3 for BrC from high-temperature biomass combustion. Besides chamber experiments, and in order to better constrain the AAE_{BrC} values that can be used in climate models, a robust observation-based estimation of AAE_{BrC} for ambient BrC PM available at many sites and over extended periods is required. Moreover, long term estimation of BC and BrC contribution to the multi-wavelength total absorption is needed to validate climate model outputs.

In this study, we used a robust experimental framework based on in-situ surface multi-wavelength absorption measurements at 44 sites in Europe to provide a unique dataset of multi-wavelength BC and BrC absorption coefficients, AAE of CA and AAE_{BrC}. Aethalometer data were used to separate BC and BrC contributions to total absorption at different wavelengths from UV to the visible (370——660 nm). At sites providing more than 8 years of data, the decadal trends for all aforementioned variables were also studied. For these stations, *meta*-analysis was performed to compare and combine the results of multiple independent studies. Unlike previous studies, which focused on singular stations or groups of stations in a single country for relatively short periods of time, our study is the first to unify across Europe the analysis of the contribution of BrC to the total absorption. This study introduces a common methodology across European stations utilizing the same measurement periods and protocol, thus enabling a proper analysis of the spatial and temporal variability of BC and BrC absorption properties. Moreover, this study presents for the first time a systematic analysis of the trends for Europe for CA absorption properties. The Aethalometer measurements used in this work were collected from different research infrastructures and/or projects, namely: RI-URBANS project (European H2020-Green Deal; https://riurbans.eu/; Savadkoohi et al., 2023), FOCI project (HORIZON-CL5-2021-D1-01; https://www.project-foci.eu/wp/), and ACTRIS (https://www.actris.eu/). The RI-URBANS and ACTRIS Aethalometer data are available in the EBAS database (https://ebas.nilu.no/). The results presented here are of special relevance to the FOCI project (Non-CO_2 forcers and their climate, weather, air quality and health impacts), which aims at reducing the knowledge gaps concerning the climate impact of many non-CO_2 radiative forcers including that of BrC PM, by examining and evaluating climate-relevant processes and feedbacks of anthropogenic primary and secondary radiative forcing species.

2. Methodology

2.1. Measurement sites

Multi-wavelength absorption data were collected at 44 measurement stations across Europe where the Aethalometer AE33 model (Aerosol Magee Scientific) was mostly deployed (39 out of 44 sites), whereas at 5 sites the older AE31 model was used. The different sites have been classified based on the information provided by the data providers as traffic (TR, 6 sites), urban (UB, 16 sites), suburban (SUB, 7 sites), regional (RB, 10 sites) and mountain (M, 5 sites) types. The station classification was used to study possible differences in BC and BrC optical properties as a function of station characteristics. A detailed description of each site, including acronym, location, Aethalometer model, measurement periods and data source is reported in Table 1. Fig. S1 shows the data coverage of each site. The data coverage (cf.

Table 1
Measurement site specifications: site, acronym, data source, latitude, longitude, altitude, measurement period, Aethalometer model, station setting. Data collection source: (*) RI-URBANS Project; (**) FOCI Project; (***) ACTRIS. (x): BUC measurement site was moved in 2020 two km away (44.34°N 26.01°E; 77 m a.s.l.). TR: traffic, UB: urban background, SUB: suburban, RB: regional background; M: mountain.

Site	Acronym	Lat.	Lon.	Alt.	Period	Aethalometer model	Station setting
Lille (FR)	ATOLL (*)	50.61°N	3.14°E	230	2017–2019	AE33	SUB
Birmingham (UK)	BAQS (*)	52.45°N	1.92°W	140	2019–2022	AE33	UB
Barcelona (ES)	BCN (*)	41.38°N	2.11°E	64	2016–2020	AE33	UB
Bern (CH)	BER (*)	46.95°N	7.44°E	536	2018–2021	AE33	TR
Birkenes (NO)	BIR (**)	58.39°N	8.25°E	219	2018–2019	AE33	RB
Bucharest (RO)	BUC (*)	44.35°N	26.03°E (x)	93	2014–2022	AE33	SUB
Carnsore Point (IE)	CASP (**)	52.17°N	6.36°W	9	2016–2017	AE33	RB
Demokritos (GR)	DEM (*)	37.99°N	23.82°E	270	2017–2020	AE33	SUB
Dublin (IE)	DUB (**)	53.31°N	6.22°W	20	2016–2017	AE33	UB
Helmos (GR)	HAC (***)	37.98°N	22.19°E	2340	2016–2019	AE31	M
Helsinki (FI)	HEL (**)	60.20°N	24.97°E	26	2016–2023	AE33	TR
Helsinki (Hakkila; FI)	HEL_H (*)	60.29°N	25.11°E	31	2018	AE33	SUB
Helsinki (Pirkkola; FI)	HEL_P (*)	60.23°N	24.92°E	20	2019	AE33	SUB
Helsinki (Rekola; FI)	HEL_R (*)	60.33°N	25.07°E	27	2017	AE33	SUB
Hohenpeissenberg (DE)	HOH (**)	47.80°N	11.01°E	985	2017–2019	AE33	RB
Hyytiälä (FI)	HYY (**)	61.85°N	24.29°E	181	2018–2022	AE33	RB
Ispra (IT)	IPR (***)	45.81°N	8.63°E	209	2007–2021	AE31	RB
Jungfraujoch (CH)	JFJ (***)	46.54°N	7.98°E	3578	2017–2019	AE33	M
Kosetice (CZ)	KOS (**)	49.58°N	15.08°E	534	2016–2018 2019	AE31	RB
Krakow (PL)	KRA (**)	50.07°N	19.92°E	383	2018–2019	AE33	UB
Ljubljana (SI)	LJB (*)	46.06°N	14.50°E	295	2019–2024	AE33	UB
Madrid (ES)	MAD (*)	40.45°N	3.72°W	669	2013–2023	AE33	UB
Marseille (FR)	MAR (*)	43.30°N	5.39°E	71	2017–2019	AE33	UB
Milano (Marche; IT)	MLN_M (*)	45.49°N	9.19°E	120	2019–2021	AE33	TR
Milano (Pascal; IT)	MLN_P (*)	45.47°N	9.23°E	120	2018–2019	AE33	UB
Milano (Senato; IT)	MLN_S (*)	45.47°N	9.23°E	120	2019–2021	AE33	TR
Montsec (ES)	MSA (***)	42.05°N	0.72°E	1570	2014–2019	AE33	M
Montseny (ES)	MSY (***)	41.78°N	2.36°E	720	2015–2020	AE33	RB
Athens-NOA (GR)	NOA (*)	37.97°N	23.72°E	105	2017–2020	AE33	UB
Observatoire Pérenne de l'Environnement (FR)	OPE (***)	48.56°N	5.50°E	392	2012–2021	AE31	RB
Paris 13ème (FR)	PA13 (*)	48.82°N	2.35°E	57	2016–2019	AE33	UB
Pallas (FI)	PAL (***)	67.97°N	24.11°E	565	2016–2021	AE31	RB
Paris (Boulevard Haussmann; FR)	PAR_B (*)	48.87°N	2.32°E	42	2016–2019	AE33	TR
Payerne (CH)	PAY (***)	46.81°N	6.94°E	489	2016–2021	AE33	RB
Puy de Dome (FR)	PUY (**)	45.77°N	2.97°E	1465	2015–2016	AE33	M
Rigi (CH)	RIG (***)	47.06°N	8.46°E	1031	2014–2021	AE33	M
Rome (IT)	ROM (*)	41.93°N	12.50°E	60	2020–2022	AE33	UB
SIRTA (FR)	SIR (*)	48.70°N	2.15°E	162	2012–2021	AE33	SUB
Stockholm (Hornsgatan) (SE)	STH_H (*)	59.31°N	18.04°E	20	2014–2023	AE33	TR
Stockholm (Torkel; SE)	STH_T (*)	59.31°N	18.05°E	45	2014–2023	AE33	UB
Tartu (EE)	TAR (**)	58.37°N	26.73°E	70	2016–2017	AE33	UB
Granada (ES)	UGR (*)	37.18°N	3.58°W	680	2014–2023	AE33	UB
Elche (ES)	UMH (*)	38.27°N	0.68°W	86	2021–2023	AE33	UB
Zurich (CH)	ZUR (**)	47.36°N	8.53°E	409	2012–2021	AE33	UB

Table 1 and Fig. S1) showcases periods spanning from over a year for short measurement campaigns (e.g. HEL_H, HEL_P, HEL_R) to around 10–15 years at stations part of aerosol monitoring networks (e.g. JFJ, IPR, ZUR, MSY). To compare the results from all sites we used hourly averaged data over a common period from 2017 to 2019. For the sites with low data coverage during 2017–2019 (BAQS, BER, CASP, DUB, LJB, MLN_M, MLN_S), we extended the period by one year. For sites without data within the considered period (ROM, PUY, UMH) the whole provided dataset was used (cf. Table 1).

2.2. Optical measurements

Aethalometer models AE31 and the AE33 (Drinovec et al., 2015) were used to measure aerosol particles light attenuation ($b_{ATN}(\lambda)$) at seven wavelengths: 370, 470, 520, 590, 660, 880 and 950 nm (cf. Table 1). In the Aethalometer, in the absence of strong dust events, the change in the attenuation with time is assumed to be caused by the increase in CA mass deposited on the filter. However, it was demonstrated that the correlation between the attenuation and the aerosol load on the filter is not linear at high attenuations (Gundel et al., 1984). Over time, the particles accumulated on the filter "shadow" each other, reducing the optical path length, saturating the signal and therefore the measurement of light transmission. This phenomenon is known as the loading effect and causes an underestimation of the true attenuation which requires a loading effect off-line correction in the case of the AE31 (e.g. Weingartner et al., 2003; Virkkula et al., 2007; Collaud Coen et al., 2010; Virkkula, 2021). The AE33 model corrects online for this artifact thanks to the dual-spot technology (Drinovec et al., 2015).

2.3. Data treatment

The Aethalometer data used in this study required different processing methods depending on the Aethalometer type and the data source. Quality-assured/quality-controlled (QA/QC) and loading effect corrected Level 2 AE31 absorption data at seven wavelengths were directly downloaded from the EBAS database (PAL, OPE, IPR, HAC). For KOS, AE31 corrected absorption data were provided by data providers. The schemes that were mostly used for loading effect correction of AE31 data were those described in Weingartner et al. (2003) and Virkkula et al. (2007). As shown by Wu et al. (2024), differences in the $b_{Abs}(\lambda)$ annual mean between AE33 and AE31 corrected with the algorithms from Weingartner et al. (2003) and Virkkula et al. (2007) are small across the seven wavelengths ($0.95 < R2 < 1$ and close-to-unity slopes between 0.87 and 1.04). The AE33 data collected in the framework of

the RI-URBANS project consisted mostly of the seven hourly-averaged eBC concentrations that were converted into harmonized absorption coefficients (b_{abs} (λ)) (in Mm^{-1}) following the procedure presented in Müller and Fiebig 2018 and Savadkoohi et al. (2023) and briefly described in Supplementary material. In the case of the AE33 data collected within the FOCI project, these consisted of raw eBC concentrations with a 1 min resolution that underwent the same data processing procedure as for RI-URBANS AE33 data and then averaged over one hour.

Finally, the AAE that describes the spectral variation of the absorption coefficients, was calculated through a linear fit of the absorption measurements over the seven wavelengths (from 370 nm to 950 nm) in the logarithmic space.

2.3.1. BC and BrC contribution to absorption

The segregation of the BC and BrC contributions to the absorption coefficient using Aethalometer measurements followed the procedure detailed in previous studies (e.g. Kirchstetter et al., 2004; Massabò et al., 2015; Liakakou et al., 2020; Zhang et al., 2020; Yus-Diez, et al., 2022) and relies on the main assumption that BrC PM do not absorb in the near-IR spectral range (880 and 950 nm). The contribution of BC particles to absorption between 370 nm and 660 nm can then be determined following Eq. (1):

$$b_{Abs,BC}(\lambda) = b_{Abs}(880nm)\left(\frac{880}{\lambda}\right)^{AAE_{BC}} \quad (1)$$

where AAE_{BC} is the AAE of the BC particles and represents the main source of uncertainty in what we call the AAE method. Indeed, many studies assumed an AAE of 1.0 for BC particles (e.g. Tian et al., 2023; Liakakou et al., 2020; Cuesta-Mosquera et al., 2024; Velazquez-Garcia et al., 2024). However, AAE_{BC} can be significantly different from 1 in the atmosphere (e.g. Bond et al., 2013; Lu et al., 2015; Costabile et al., 2017) as it depends on morphology, size distribution, sources and mixing state of BC particles. Here we estimated the AAE_{BC} at each site as the 1st percentile of the calculated AAE. Since, the contribution of BrC to absorption increases the AAE, the 1st percentile represents conditions where the absorption can be assumed to be dominated by BC particles. In order to reduce the noise, the 1st percentile at each site was determined from AAE values obtained from fits with $R^2 > 0.99$ (Tobler et al., 2021). Fig. S2 shows the AAE frequency distributions and AAE_{BC} estimations using the R^2-filtered AAE (calculated from 370 to 950) at the 44 sites. It should be noted that this is the first time that the 1st percentile of the AAE frequency distribution has been systematically used across multiple measurement stations to estimate the AAE_{BC}. The AAE_{BC} calculations were performed using data collected from 2018 onwards, when the recommended M8060 filter tape was introduced.

At sites where the AE33 was deployed, the 1st percentile provided AAE_{BC} values from 0.88 to 1.12, with 85 % of the values lying in the 0.9–1.1 range which has been associated to BC from fossil fuel combustion (e.g. Bond et al., 2006; Zotter et al., 2017; Blanco-Allegre et al., 2020). Exceptions were DUB, CASP, JFJ, HYY and STH_H where the 1st percentile provided AAE_{BC} values that were considered too low to properly represent the AAE of BC particles. The reasons for these low 1st percentiles are unknown. At the JFJ and HYY remote sites low percentiles could be related to the low signal-to-noise ratio of Aethalometer signals, especially in the near-IR, thus increasing the noise of the calculated AAE and consequently affecting the calculation of the 1st percentile. However, calculating the 1st percentile using only b_{abs} (λ) higher than 0.1 Mm^{-1} did not contribute to increasing the 1st percentile. CASP and DUB are sites where strong contribution to PM from marine aerosols has been observed (Chen et al., 2022), that could have considerably increased the SSA of the particles collected on the filter tape. An excessive SSA could affect b_{abs} (λ) and thus also the calculated AAE (Yus-Diéz et al., 2022). STH_H is a traffic site heavily influenced by traffic emissions (e.g. Savadkoohi et al., 2023), where the presence of fresh and small BC particles could be expected whereas the low calculated AAE_{BC} (0.83) suggested the predominance of bigger BC particles (e.g. Wang et al., 2016). Moreover, at the UB site in the same city (STH_T) a 1st percentile of 1.02 was obtained. For all these sites with extremely low 1st percentile values an AAE_{BC} of 1 was used in Eq. (1). In addition, the AE31 instruments provided systematically low percentiles compared to AE33 ranging from 0.55 to 0.71 with the exception of IPR where 0.85 was calculated. In these cases, a value of 1 was also used in Eq. (1).

The method applied here for the determination of the contribution to total absorption from BrC PM is prone to high uncertainties especially at sites where the measured absorption was low. Kalbermatter et al. (2022) reported measurement uncertainties of the AE33 including the cross-sensitivity to scattering (Yus-Díez et al., 2021) to be around 20 % which was consistent with the 25 % value from the WMO/GAW (2016). Moreover, we estimated, similarly to Zhang et al. (2020), an uncertainty of around 10 % in the estimation of $b_{Abs,BC}(\lambda)$ for a +/-10 % variation from the used AAE_{BC} values. Based on these uncertainties estimation, the overall uncertainty of the calculated absolute values of $b_{Abs,BrC}(\lambda)$ reported here was considered to be not lower than around 20–25 %.

Once the AAE_{BC} was determined, the contribution of BrC to the total absorption between 370 nm and 660 nm was estimated by subtracting the absorption due to BC to the measured total absorption (Eq. (2).

$$b_{Abs,BrC}(\lambda) = b_{Abs}(\lambda) - b_{Abs,BC}(\lambda) \quad (2)$$

Then, the AAE of BrC (AAE_{BrC}) was similarly calculated as the linear fit in the log–log space ($b_{Abs,BrC}$ vs. wavelength), but between 370 and 660 nm, since BrC presents no absorption in the near-IR part of the spectrum. To interpret its variability we also calculated AAE_{BrC} between ranges 370–520, 370–590, and 590–660 nm.

2.3.2. Effect of dust absorption

Dust particles can also absorb radiation and contribute to the Aethalometer signal in the UV/near-IR spectrum (880 and 950 nm in this case). They are brownish/orange and feature a similar wavelength dependence of absorption than BrC. Moreover, due to their high SSA, dust particles can increase the apparent absorption provided by the Aethalometer by increasing the apparent multiple-scattering parameter C (Yus-Díez et al., 2021). These phenomena hamper the application of the AAE method and the determination of $b_{Abs,BrC}(370)$ during Saharan dust events (SDE) which regularly affect Southern European sites (Alastuey et al. (2016)). Due to the low absorption efficiency of dust compared to BC and BrC, a non-negligible contribution of dust to absorption is only expected if large amounts of dust are transported from North African dust source areas to the European surface, especially at remote sites where the mass concentration of BC and BrC is on average low. For example, Pandolfi et al. (2014b) and Bukowiecki et al. (2016) reported that long-range transport of dust occurs rather frequently at the MSA and JFJ mountain sites with a non-negligible effect on aerosol properties during extreme events. Conversely, at traffic, UB and even RB sites at Central-Northern Europe the effect of dust on absorption is usually neglected compared to that of BC and BrC PM. In this study, we used the information available at some Mediterranean (BCN, MSY, MSA, UGR, DEM) and remote (JFJ and HAC) sites to detect SDE and filter out the dust days. For the Spanish sites of BCN and MSY, the methodology used to identify the Saharan dust days has been described in detail (e.g. Querol et al., 2019) and was performed using different dust concentration and transport model outputs and meteorological information. This methodology has been officially accepted by the European Commission for reporting on natural contributions to ambient PM levels over Europe and was applied here (EC, 2011). For the Greek stations of DEM and HAC, for JFJ (Switzerland) and for UGR and MSA (Spain) the Ångström exponent of the single scattering albedo SSA (SSAAE) was calculated from aerosol particles scattering and absorption data (EBAS for scattering; https://www.ebas.nilu.no; last access 15/07/2024) and used to

filter out dust days. The SSA is the ratio between the scattering and the extinction coefficients and the wavelength dependence of the SSA can be characterized with its exponent which depends on the absorption (AAE) and scattering (SAE) Ångström exponents: SSAAE = (1-SSA)·(SAE-AAE) (Moosmüller and Chakrabarty, 2011). SSAAE provides information about the type of sampled aerosols and it has been proposed as a good indicator for the presence of Saharan dust in the atmosphere (Collaud Coen et al., 2004; Ealo et al., 2016), in fact, the presence of Saharan dust particles causes a reduction of the SAE and an increase of AAE, resulting in negative SSAAE values during these events. Collaud Coen et al. (2004) reported for the JFJ measurement site that the SSAAE was able to detect 100 % of Saharan dust outbreaks compared with 80 % and 40 % of events detected using SAE and AAE respectively.

2.3.3. Trend analysis

We performed a trend analysis at sites where a minimum of 8 years of data was available. This was the case for 12 monitoring sites. We analyzed the trends of total absorption, BC and BrC absorption at 370 nm, the relative contribution of BrC to total absorption, the AAE of CA and the AAE of BrC. The monitoring sites included in this analysis are: HEL (2016–2023), STH-H (2015–2023), UGR (2014–2023), ZUR (2012–2023), MAD (2013–2023), STH-T (2015–2023), BUC (2014–2022), SIR (2012–2021), IPR (2007–2021), MSY (2015–2023), OPE (2012–2021), and RIG (2014–2021).

Trend analyses were performed using the methodology proposed by Collaud Coen et al. (2020). This approach involves applying the Mann–Kendall non-parametric method with Sen's slope estimator (Gilbert, 1987; Kendall, M., 1975; Mann, H. B., 1945; Sirois, 1998). To consider the effect of autocorrelation and time granularity, the algorithm incorporates three prewhitening methods that guaranteed the robustness of the identified trends (Collaud Coen et al., 2020). To compute the trends, the 3PW R package (Bigi and Vogt, 2021) was used. Details on the implementation the 3PW method can be found in the study by Collaud Coen et al. (2020) and in the mannkendall/R package (https://mannkendall.github.io/, last access 6 August 2024).

To evaluate both the overall trends and those specific to the different site classifications (traffic, urban, suburban, regional, and mountain) we performed several *meta*-analyses to account for the heterogeneity observed among the sites (Balduzzi et al., 2019). Individual slopes, representing the percentage change per year along with their 95 % confidence intervals, were analyzed using random-effects *meta*-analysis (Zeng and Lin, 2015). Mean effects were calculated both separately for each site type as well as globally, to offer a comprehensive overview. The *meta*-analyses were performed using the "*meta*" R package version 7.0–0 (Schwarzer et al., 2015).

3. Results

3.1. Absorption at 370 nm: Regional and site type differences

Figs. 1 and 2 provide an overview of $b_{Abs}(370)$ at the 44 stations across Europe. Here we focus on $b_{Abs}(370)$ where the contribution of CA particles to absorption was the highest. Overall, northern countries showed on average lower absorption compared to central/southern countries, as also recently reported for BC concentrations in Europe by Savadkoohi et al. (2023). Moreover, on average, higher absorption was observed in Central and Eastern Europe compared to Western Europe. Fig. 1 highlights that the spatial coverage of measurement stations was higher in the Western and Central countries compared to Eastern countries, a limitation that may affect the comprehensive assessment of the spatiotemporal variability of absorption across Europe. Fig. 2 shows that the most important parameter affecting the measured $b_{Abs}(370)$ was the station setting, causing a clear gradient with values increasing from mountain to urban and traffic sites. The observed high site-by-site variability within each station category can be mostly associated with site location, CA sources strength and meteorological patterns, as well as secondary aerosols production.

At mountain sites, the station altitude influenced the measured absorption values. For example, median $b_{Abs}(370)$ values ranged from 8.89 Mm^{-1} at PUY measurement site (1465 m a.s.l.) down to 0.24 Mm^{-1} at JFJ, the high altitude (3578 m a.s.l.) site. However, the distance from important CA sources and the topographic features of the mountainous regions likely played the most important role in determining the level of measured $b_{Abs}(370)$. For example, Collaud Coen et al. (2018) have

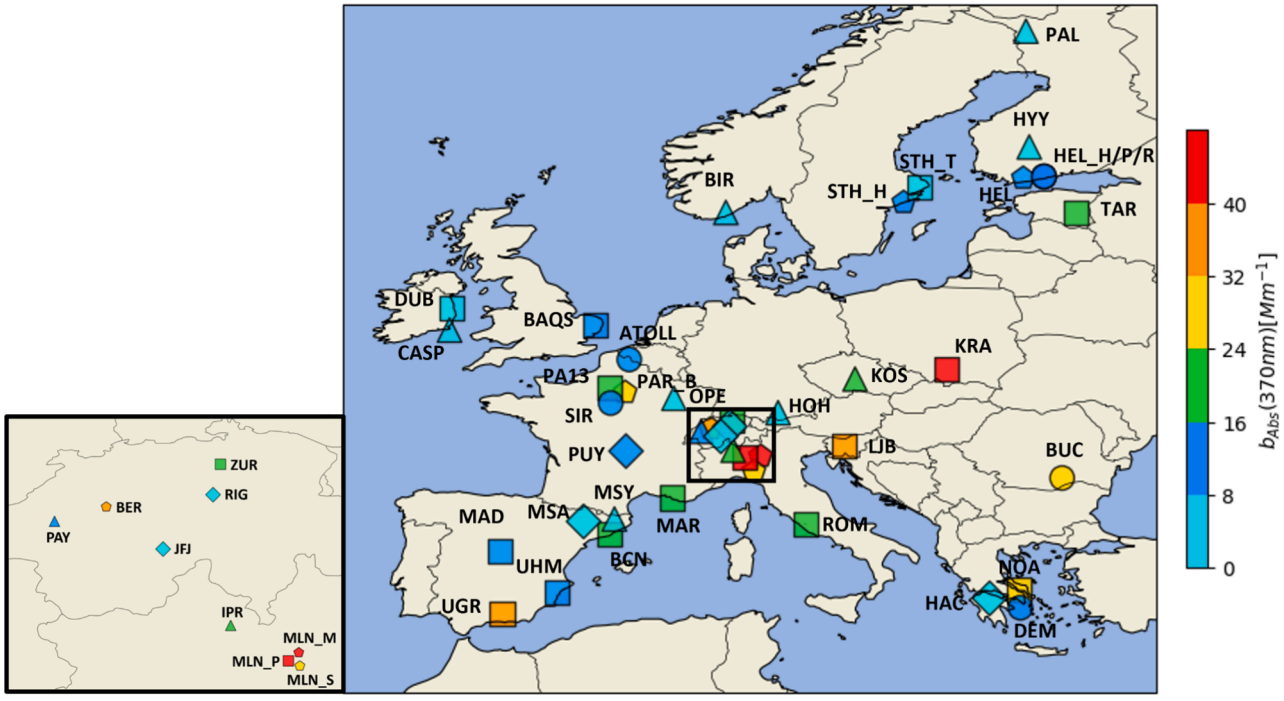

Fig. 1. Map with the mean total absorption at 370 nm at all stations organized by their settings: traffic (pentagon), urban (square), suburban (circle), regional (triangle) and mountain (rhombus). Period: 2017–2019.

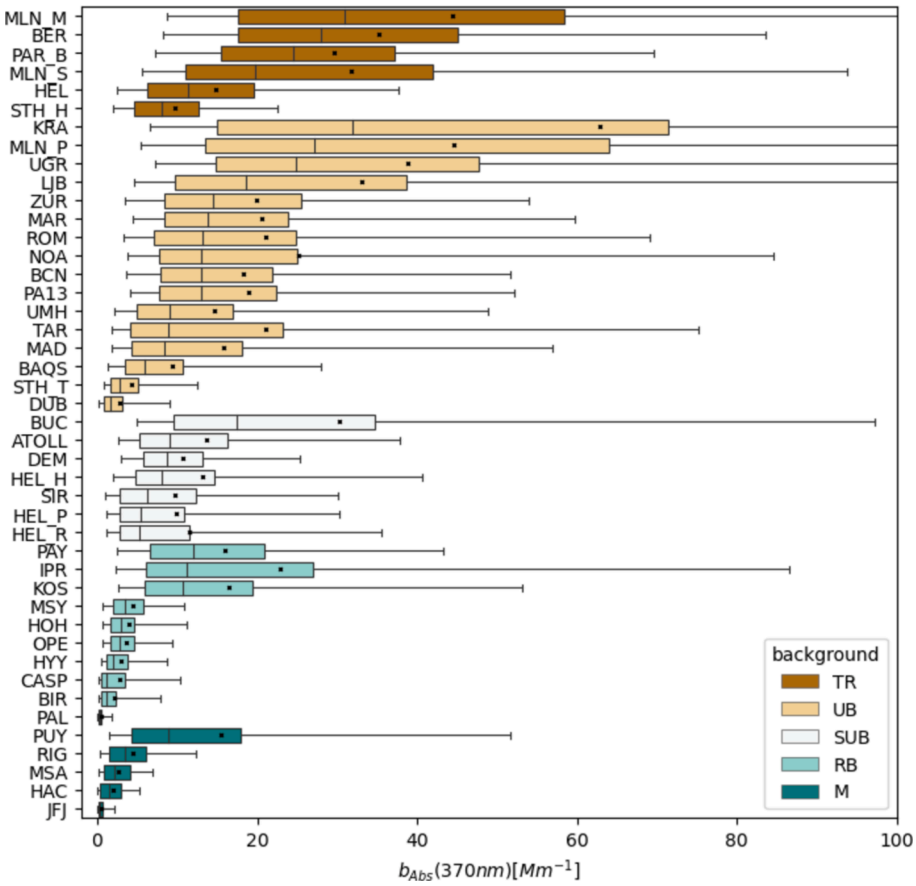

Fig. 2. Box plots (5th, 25th, 50th, 75th, 95th percentiles) of total absorption at 370 nm sorted by station settings: dark green (mountain sites), light green (regional background sites), white (suburban sites), orange (urban background sites), brown (traffic sites). Black lines and dots in each box-whiskers-plot represent the median and mean values, respectively. Period: 2017–2019.

shown that the MSA site, located approximately at the same altitude as PUY (cf. Table 1), is less affected than PUY by the pollution within the atmospheric boundary layer (ABL) and, consequently, the $b_{Abs}(370)$ at MSA was much lower compared to PUY (cf. Fig. 2). Correspondingly, the very low $b_{Abs}(370)$ measured at JFJ and HAC agreed with the very low influence of ABL at these two sites as shown in Collaud Coen et al. (2018). For regional stations, a high variability of $b_{Abs}(370)$ related mostly to the location of the measurement sites was observed. At PAL, a remote regional site, the median $b_{Abs}(370)$ was 0.25 Mm^{-1} whereas it lies between 10.66 and 11.99 Mm^{-1} at IPR, KOS and PAY. IPR is located in the Po Valley, one of the most polluted regions in Europe, characterized by extremely low winds and frequent atmospheric stagnation episodes in winter favoring the accumulation of pollutants (e.g. Gilardoni et al., 2020; Savadkoohi et al., 2023). Similarly, meteorology in winter also plays an important role in the accumulation of pollutants at the PAY site located on the Swiss plateau with a high average population density. Recently, Chen et al. (2022) have shown that the submicron particulate matter mass concentration (PM_1) at the regional KOS site was comparable and even higher compared to European urban sites. Moreover, the accumulation in winter of CA from combustion sources as traffic and biomass burning contributed to explain the relatively high absorption measured at KOS (Chen et al., 2022). At these three RB sites, the measured absorption was higher compared to the SUB sites with the exception of BUC. The $b_{Abs}(370)$ measured at IPR, KOS and PAY was also higher compared to some UB and TR sites reflecting the importance of regional pollution and meteorology, which influence the transport of pollutants and production of secondary aerosols. With regards to BUC, this site showed significantly higher $b_{Abs}(370)$ than other suburban stations, primarily due to its higher BC concentrations compared to similar sites in other regions (Savadkoohi et al., 2023). The site-by-site variability of $b_{Abs}(370)$ at UB and TR sites was also very high. In general, the observed variations at UB sites ranged from very low $b_{Abs}(370)$ around 1.59–2.85 Mm^{-1} at DUB and STH_T to high values of 24.32–31.85 Mm^{-1} at KRA, MLN_P and UGR. A similar trend was also reported for BC concentrations by Savadkoohi et al. (2023).

KRA is considered to be a pollution hotspot in Europe (e.g. Samek et al., 2019; Tobler et al., 2021; Casotto et al., 2023) where the high consumption of coal and wood for energy production and residential heating together with specific meteorological and topography features contributed to make KRA the site with the highest $b_{Abs}(370)$ among the 44 sites included in this work. The data for KRA in this study covered the period January 2018 – April 2019, prior to the September 2019 ban on using solid fuels (coal and wood) in boilers, stoves or fireplaces. It should also be noted that the OM concentrations measured in KRA during the same period reported here were also the highest among the European measuring sites included in Chen et al. (2022). UGR also exhibited high $b_{Abs}(370)$, 24.32 Mm^{-1}, likely due to its location in a depression at the foot of Sierra Nevada mountains with frequent thermal inversion during the cold months, causing biomass burning and traffic emissions to accumulate (Lyamani et al., 2011; Titos et al., 2017). The UB MLN_P site also recorded high $b_{Abs}(370)$ values (27.12 Mm^{-1}), similar to the two traffic sites in Milan (MLN_M: 31.01 Mm^{-1} and MLN_S: 19.67 Mm^{-1}). Milan, located in Po Valley, is a high-density polluted area, similar to Paris (PAR_B: 24.58 Mm^{-1}), one of the largest cities in Europe. These urban sites feature higher absorption values compared to stations like in HEL (11.42 Mm^{-1}) and STH_H (7.99 Mm^{-1}), which are located in less populated areas with lower emissions and with meteorological patterns that favor the dispersion of local pollutants (Savadkoohi et al., 2023).

3.2. Contribution of BC and BrC to absorption at 370 nm

Fig. 3 illustrates the variability among the measurement sites for $b_{Abs,BC}(370)$ and $b_{Abs,BrC}(370)$ (Fig. 3a and 3b, respectively), as well as the relative contribution of BrC to total absorption (Fig. 3c). As aforementioned, we focus on the absorption at 370 nm where the relative contribution of BrC is the highest compared to other wavelengths. Fig. S3 presents the relative contribution of BC and BrC to total absorption from 370 to 660 nm.

Overall, both $b_{Abs,BC}(370)$ and $b_{Abs,BrC}(370)$ showed a similar gradient as observed for $b_{Abs}(370)$, with values increasing from mountain to urban/traffic sites and with high variability at each measurement site. A strong site-by-site variability within each station setting was also observed. This similarity in the $b_{Abs,BC}(370)$ and $b_{Abs,BrC}(370)$ trends is related to the fact that the main BC sources also emit primary organic aerosols (POA), which can have a large range of absorption efficiencies depending on both the fuel used and the combustion conditions. In addition to biomass burning, fossil fuel, biofuel and coal combustion have also been identified as significant sources of both primary and secondary BrC PM (Yang et al., 2024; Corbin et al., 2018; Ni et al., 2021, among others). Recent field and laboratory studies have highlighted the light-absorbing properties of internal combustion engine BrC sources such as vehicular emissions (e.g. Kaskaoutis et al., 2021; Chen et al., 2020; Saleh et al., 2014; Zhang et al., 2020; Qin et al., 2018; Kasthuriarachchi et al., 2020; Saleh et al., 2020). For instance, Saleh et al. (2018) performed controlled-combustion experiments using benzene and toluene as fuels and observed that, depending on the combustion conditions, the color of the resulting BrC components ranged from light to dark. Along with some contribution from solid fuel combustion, this could explain the non-negligible $b_{Abs,BrC}(370)$ observed at traffic sites (cf. Fig. 3b, c).

The relative contribution of $b_{Abs,BrC}(370)$ to $b_{Abs}(370)$ (%Abs_{BrC}; for the 2017–2019 period; cf. Fig. 3c) was, as expected, on average lower at traffic sites (median values around 11–21 %). However, a clear difference between UB, SUB, RB and M sites was not observed for % Abs_{BrC}, suggesting that, apart from traffic sites, the station setting was not the main parameter determining the relative contribution of BrC to absorption. Overall, the mean %Abs_{BrC} did not show a clear spatial gradient with occurrence of low and high values observed in each country (Fig. S4). However, on average, the occurrence of low %Abs_{BrC} was observed mostly in Western/Central Europe whereas in Eastern countries the average %Abs_{BrC} was higher, likely reflecting a stronger contribution of primary and secondary BrC sources, such as biomass burning and coal combustion (e.g. Chen et al., 2022). These differences were however not statistically significant, likely due to the lower spatial data coverage in the East compared to western/central Europe. These similar contributions (except at sites directly impacted by traffic) can be attributed to two causes: primary BrC due to homogeneous distribution of sources; or dominant contribution of secondary BrC, which is more homogeneously distributed in the boundary layer (Zhang et al., 2015, Su et al., 2018; Li et al., 2021). It should be noted however that the spatial coverage of available data in each country could have affected the presented analysis. The %Abs_{BrC} values reported here were consistent with those reported in the literature for some of the sites included in this work where an AAE_{BC} of 1 was mostly used. On the other hand, Zhang et al. (2020) have reported an uncertainty of approximately 11 % in the estimation of the $b_{Abs,BrC}(370)$ contribution to $b_{Abs}(370)$ when using different AAE values ranging from 0.9 and 1.1. For example, for NOA Kaskaoutis et al. (2021) reported a mean $b_{Abs,BrC}(370)$ contribution to $b_{Abs}(370)$ of 44 % during winter 2016–2017 very close to the mean value calculated in this work of 40 % for the same period. For the same NOA site, Liakakou et al. (2020) presented a mean contribution of $b_{Abs,BrC}(370)$ of around 24 % for a longer period (2015–2019) that closely matched our estimation of 21 % (2017–2019). For the ATOLL, SIRTA and MAR French sites, $b_{Abs,BrC}(370)$ contributions of 22, 42 and 18 %, respectively, were reported by Velazquez-Garcia et al. (2023) and Zhang et al. (2020), close to the estimations reported here of 20, 40 and 18 %, respectively, for the same sites and periods. The contribution of

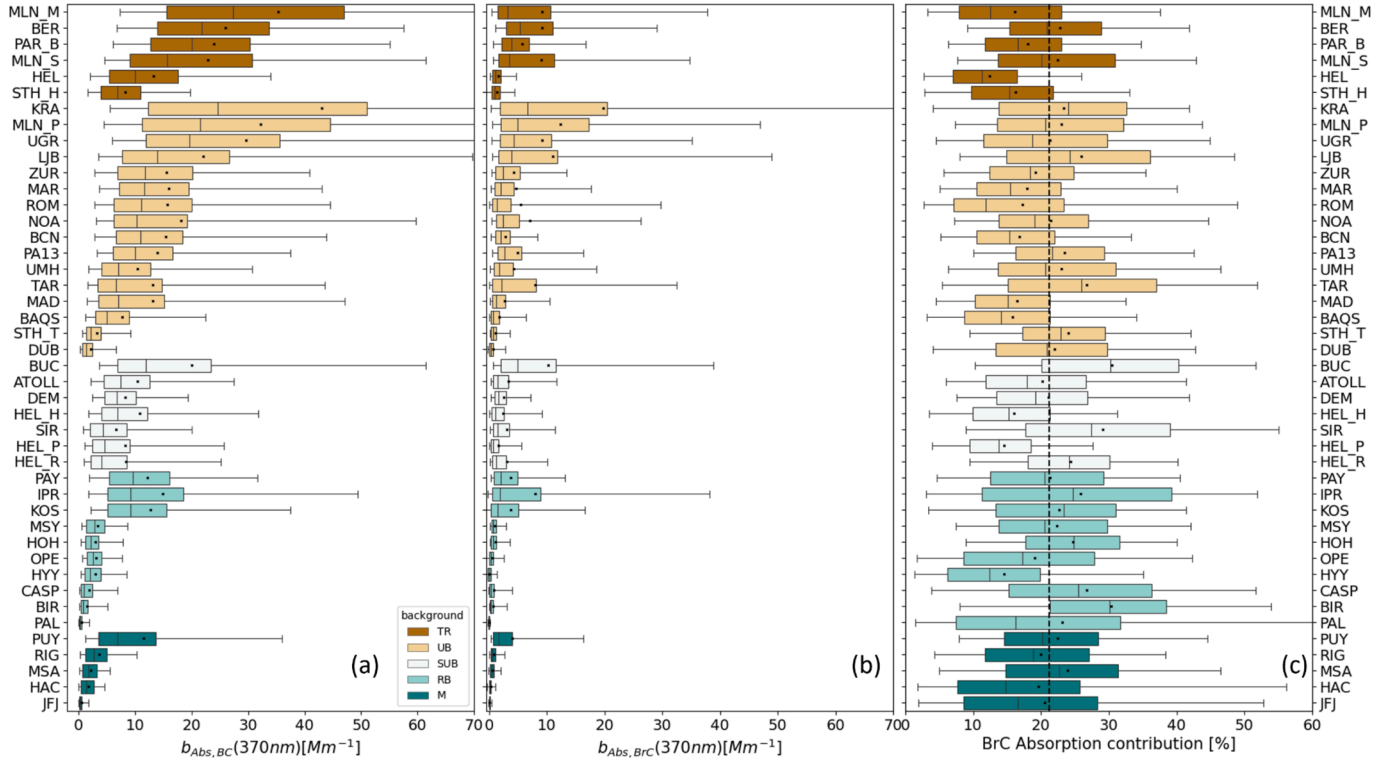

Fig. 3. The same as in Fig. 2 for $b_{Abs,BC}(370)$ (a), $b_{Abs,BrC}(370)$ (b) and the relative BrC contribution to $b_{Abs}(370)$ (c). Vertical dashed line represents the mean calculated for all sites. Period: 2017–2019.

$b_{Abs,BrC}(370)$ to $b_{Abs}(370)$ of 31 % reported here for UMH Spanish site in winter was also very close to the estimation of 34 % reported by Lopez-Caravaca et al. (2024). The similitude in the values reported here and in the literature showcases the validity of the method, the representativeness of the period used in this study, and the feasibility of comparing the presented results among the sites used here.

3.3. AAE and AAE_{BrC} variability

Fig. 4 shows the AAE valuescalculated from the absorption measurements between 370 and 950 nm and the AAE_{BrC} calculated from the estimated BrC absorption between 370 and 660 nm. At all sites the AAE_{BrC} was considerably higher than AAE as a consequence of the stronger wavelength dependence of absorption by BrC than by BC, which together add up to total absorption by CA.

As shown in Fig. 4, the lowest AAE values were observed at the traffic sites (TR) for the whole subgroup and, even if highly heterogeneous, the AAE variability was more pronounced compared to the site-to-site variability observed for $\%Abs_{BrC}$ (cf. Fig. 3c) showing however similar behavior, with high/low AAE associated with high/low $\%Abs_{BrC}$. Lower median AAE values around 1.1 were observed at MLN_M, PAR_B and STH_H traffic sites, at HYY and PAL regional sites, and at the high altitude JFJ mountain site. Consequently, apart from traffic sites, the lowest median AAE values were also observed at the more remote RB and M sites. This could be due to the lack of proximity from primary BrC sources as well as the effect of photobleaching and whitening of BrC during transport toward these remote sites (Fleming et al.,2020; Li et al., 2023; Fang et al., 2023). At the other RB sites and low altitude mountain sites the median AAE was on average higher reflecting a higher influence of BrC sources. High median AAE values (>1.3) were observed at some urban sites (KRA, LBJ and TAR), SUB sites (BUC, SIRTA and HEL_R), RB sites (PAY, KOS, HOH and IPR) and at the RIG low mountain site. Independently of the station location, Western Europe showed AAE values mostly below 1.3 whereas in the east it increased to values higher than 1.3 (Fig. S4) likely due to the higher relative contribution to BrC due to a more extensive use of coal and biomass burning (e.g. Chen et al., 2022). The same regional pattern was not observed for the AAE_{BrC}. In fact, this parameter seemed to be rather independent on both regional location (Fig. S4) and station background (cf. Fig. 4b). Notable exceptions were the RB sites, with the exception of PAY, and the cleanest sites (JFJ, HAC and PAL) where the median AAE_{BrC} values were on average lower compared to the median calculated using all the sites (cf. Fig. 4b).

Based on the information available here, it is not straightforward to understand the observed variability of AAE_{BrC} since this parameter depends on the physico-chemical properties of BrC PM and on the transformation processes, including browning and photobleaching, of BrC during transport.

Previous studies based mostly on smog chamber experiments, (e.g. Lambe et al., 2013; Saleh et al. 2013, 2014; Kumar et al., 2018) have shown that SOA particles, especially those produced in aged biomass burning emissions, can be more absorptive in the UV and short visible range (370–590 nm) than in the long visible (660 nm) and exhibit stronger wavelength dependence than POA. Thus, these studies have shown that the AAE_{BrC} of the less absorbing SOA is higher compared to the AAE_{BrC} of the more absorbing POA. Consequently, a relative increase of SOA from biomass burning in OM particles could cause an increase of the observed AAE_{BrC}. In order to interpret the variability of AAE_{BrC} reported in Fig. 4b we compared the AAE_{BrC} calculated from 370 to 660

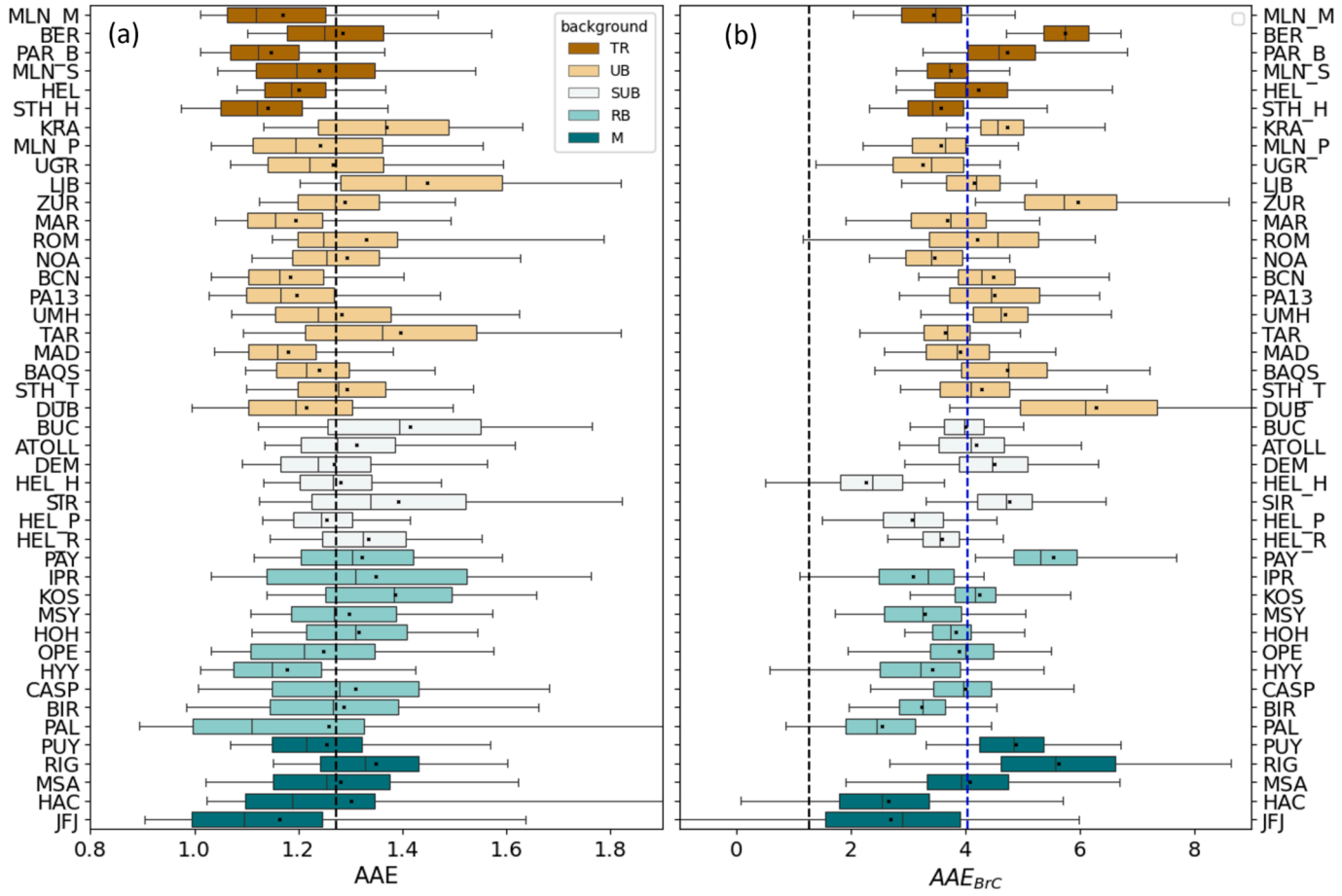

Fig. 4. The same as in Figs. 2 and 3 for CA AAE between 370 and 950 nm (a) and of AAE_{BrC} from 370 to 660 nm (b). Black dashed vertical lines represent the mean AAE and the blue dashed vertical line in (b) shows the mean AAE_{BrC}.

nm with the AAE_{BrC} calculated from 370 to 590 nm. The results of this analysis are reported in Fig. S5. Fig. S5a shows that for the majority of the sites the AAE_{BrC} (370–660 nm) was higher compared to the AAE_{BrC} (370–590 nm). The higher AAE_{BrC} (370–660 nm) was due to a strong relative decrease of the absorption by BrC PM in the long visible (660 nm) compared to the UV/short-visible (370–590 nm), as illustrated in Fig. S5b for the example of BER. The observed general decrease of BrC absorption at 660 nm was also demonstrated by the fact that the difference considering all the sites between AAE_{BrC} (370–590 nm) and AAE_{BrC} (370–520 nm) was small and around 0.13 ± 0.22. This relative decrease of Abs_{BrC} from the long visible onwards compared to the UV/short-visible range has been observed in other studies for samples containing a substantial contribution of organic species and point out that the AAE_{BrC} depends on the range of wavelengths selected for its calculation (Harrison et al., 2013; Utry et al., 2014; Cuesta-Mosquera 2021, 2024).

3.4. Seasonal variability

Fig. 5 shows the normalized annual cycles calculated with feature scaling for the 2017–2019 period of $b_{Abs}(370)$, $b_{Abs,BC}(370)$, $b_{Abs,BrC}(370)$, $b_{Abs,BrC}$ relative contribution to $b_{Abs}(370)$, AAE and AAE_{BrC}.

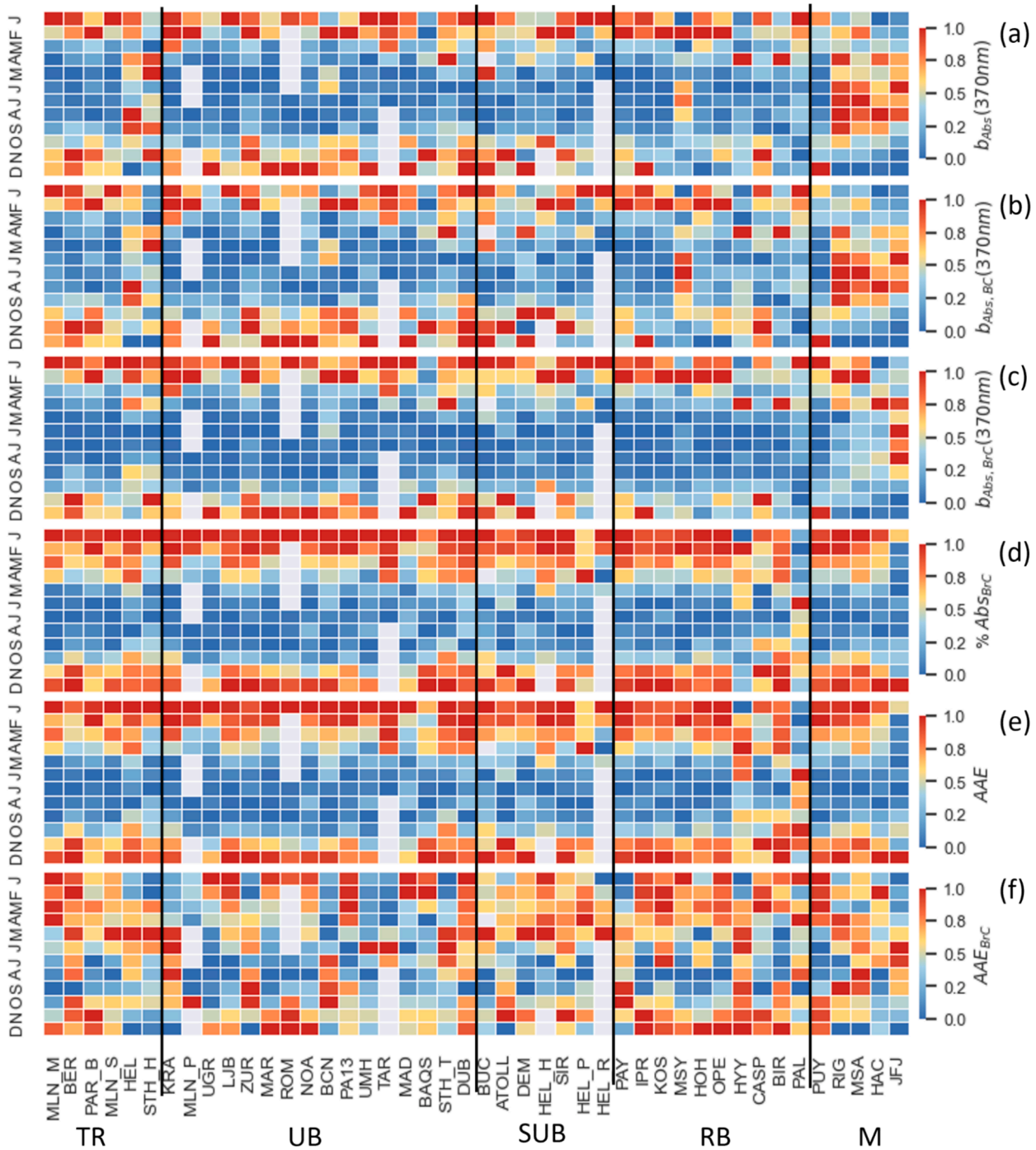

Fig. 5. Normalized annual cycles of total absorption at 370 nm (a; $b_{Abs}(370)$), BC contribution to total absorption (b; $b_{Abs.BC}(370)$), BrC contribution to total absorption (c; $b_{Abs.BrC}(370)$), relative contribution of BrC to total absorption (d; $\%Abs_{BrC}$), AAE of CA from 370 to 950 nm (e), and AAE of BrC from 370 to 660 (f). Color code 0–1 indicates progressive increase from lowest value (blue) to highest value (red).

The absolute values for each variable are reported in Table S1. Fig. 5 shows that apart from AAE_{BrC}, both the relative and absolute values of the presented variables increased in winter at all low-middle altitude sites and decreased on average in summer. The observed increases in winter could be attributed to both the seasonal variability of CA emission sources and meteorological conditions. In fact, winter periods are characterized by higher emissions due to heating and by lower atmospheric boundary layer heights, lower wind speeds and enhanced atmospheric stability which contribute to the greater accumulation of pollutants. Conversely, in summer the atmospheric conditions favor the dispersion of pollutants due to higher atmospheric boundary layer heights and higher wind speed. Notable exceptions were the mountain sites where the higher dispersion in summer associated with thermally driven winds allowed the transport of pollutants toward these elevated sites thus increasing both the $b_{Abs}(370)$ and the $b_{Abs,BC}(370)$ during the warm season (e.g. Putaud et al., 2004, 2010; Pandolfi et al., 2014a; 2018; Viana et al., 2016; Collaud Coen et al., 2018; Zhang et al., 2020; Yttri et al., 2021). At these elevated sites the relative increase in summer of $b_{Abs,BrC}(370)$ was less pronounced compared to $b_{Abs,BC}(370)$ with the exception of the very elevated JFJ mountain site. A similar summer trend for $b_{Abs}(370)$ and $b_{Abs,BC}(370)$ was also observed at the MSY regional site (720 m a.s.l.) located in an elevated regional area (e.g. Pandolfi et al., 2014b).

The lack of a clear relative increase of $b_{Abs,BrC}(370)$ in summer at the elevated sites can be mostly associated with the reduction of BrC emissions from sources such as biomass burning during the warm season (e.g. Cordell et al., 2016; Putaud et al., 2018; Casquero-Vera et al., 2021), lower emissions of precursors available for coating of BC (e.g. Yuan et al., 2020) and photobleaching associated with enhanced solar irradiation in summer (e.g. Dong et al., 2024; Paraskevopoulou et al., 2022). For $b_{Abs}(370)$ and $b_{Abs,BC}(370)$ relative increases in summer were also observed at northern traffic sites (HEL and STH_H). Similar increases in summer at these Nordic sites were reported for eBC concentrations by Savadkoohi et al. (2023) and attributed to the fact that these two sites are located in street canyons, thus making the local traffic the dominant source of CA throughout the year. Similarly to Fig. 5b and 5c, Barreira et al. (2021) reported for HEL an increase of the traffic contribution to eBC concentrations and a decrease of biomass burning contribution to eBC in summer partly explained by poorer dispersion and lower ventilation factor especially during August. Seasonal variations at the STH_H site can also be affected by the abatement of traffic since traffic exhaust has been found the most important source in the city of Stockholm (Segersson et al., 2017).

The relative contribution of $b_{Abs,BrC}(370)$ to $b_{Abs}(370)$ ($\%Abs_{BrC}$ in Fig. 5d) increased at all sites in winter indicating that the relative increase in winter of BrC absorption was higher compared to the absorption due to BC particles. This was mostly related to the increase of BrC emissions and emissions of their precursors during the cold months from specific sources such as residential wood burning (e.g. Zhang et al., 2020; Zalzal et al., 2024). As shown in Fig. 5d and Table S1, in winter the relative contribution of $b_{Abs,BrC}(370)$ to $b_{Abs}(370)$ frequently reached values up to more than 40 % demonstrating the high potential of BrC PM to contribute to the measured $b_{Abs}(370)$. Moreover, this strong relative increase during the cold period was independent of the station background. The exception was PAL, a remote RB site, where the $\%Abs_{BrC}$ was relatively higher in summer. At PAL the very low seasonal variability on the $b_{Abs,BrC}(370)$ (0.1–0.2 Mm^{-1}; cf. Table S1) suggested that the $\%Abs_{BrC}$ depended exclusively on the seasonal variability of the $b_{Abs,BC}(370)$ (0.2–1.1 Mm^{-1}; cf. Table S1) with higher (lower) $b_{Abs,BC}(370)$ contribution to $b_{Abs}(370)$ causing a decrease (increases) of the relative contribution of $b_{Abs,BrC}(370)$ to $b_{Abs}(370)$. Consistently with the relative contribution of $b_{Abs,BrC}(370)$ to $b_{Abs}(370)$, the AAE also showed a clear increase in winter at all sites with the exception of PAL where higher AAE values were observed in summer. Finally, no clear seasonal pattern was observed for the AAE_{BrC}, indicating that the wavelength dependence of BrC absorption was not related to the seasons.

3.5. Diel variability

Fig. 6 shows the normalized, with feature scaling, diel cycles calculated for the period 2017–2019 for the different variables considered in this work. The mean absolute hourly values for each variable are reported in Table S2. Overall, the $b_{Abs,BC}(370)$ (cf. Fig. 6b) followed the typical bimodal diel pattern influenced by anthropogenic activities with maxima during the morning (traffic rush hour between 06:00–09:00) and evening hours (17:00–21:00, traffic rush hour and cooking and heating activities), and a decrease during midday mostly due to atmospheric dilution and, to a lesser extent, the reduction of BC emissions. Exceptions were the mountain sites where both $b_{Abs}(370)$ and $b_{Abs,BC}(370)$ increased at noon under higher mixing layers and stronger thermal wind systems favoring the dilution and transport of pollutants from the lower-lying source regions toward these elevated sites during the warmest hours of the day.

Overall, $b_{Abs,BrC}(370)$ showed different diel cycles compared to $b_{Abs,BC}(370)$, lacking the morning rush-hour peak, with higher $b_{Abs,BrC}(370)$ observed at night mostly related to BrC emissions from domestic activities such as heating (e.g. Zhang et al., 2020). Conversely, $b_{Abs,BrC}(370)$ was lower in the morning due to the decrease of these household activities. The $b_{Abs,BrC}(370)$ at the traffic sites followed more closely the diel cycles of $b_{Abs,BC}(370)$ likely because of the lack of a strong contribution to BrC from household activities and the fact that vehicles can also contribute to BrC PM through emissions and/or coating of BC secondary organic material. Consistently, both the relative contribution of $b_{Abs,BrC}(370)$ to $b_{Abs}(370)$ ($\%Abs_{BrC}$ on Fig. 6d) and the AAE (Fig. 6e) showed similar diel cycles with increases at night.

In contrast to the annual cycles, a rather clear AAE_{BrC} diel cycle was observed with lower values during the day and higher values at night and early morning. This could indicate the formation of specific brown SOA (particles or coatings on existing primary particles) at night with stronger wavelength dependence in the UV/short visible. For example, previous studies have reported that a possible pathway of BrC formation at night is the nitrate radical (NO_3)-initiated oxidation of specific compounds in the presence of NO_2 and NO_x, and have identified wood burning and traffic as the most important sources of BrC SOA particles (e.g. Wang et al., 2019; Frka et al., 2022). A second possibility is condensation of secondary organic material on existing primary particles, especially BC (Kalbermatter et al., 2022). It should be considered that the possible photobleaching of BrC particles during the day could also have affected the reported diel cycles (Fleming et al.,2020; Li et al., 2023).

3.6. Trend analysis of CA absorption properties

For trend analysis, we used data from a subset of 12 measuring sites that provided at least 8 consecutive years of data using the same Aethalometer model and the trends were considered as statistically significant (s.s.) only for p-values lower than 0.01. This choice was supported because a p-value < 0.01 has been found to be more robust than the commonly used p-value threshold of 0.05 (Vidgen and Yasseri, 2016).

The meta analysis including all sites presented in Fig. 7 shows that overall $b_{Abs}(370)$ decreased by 1.57 %/year driven by a decrease of $b_{Abs,BC}(370)$ (2.01 %/year), whereas $b_{Abs,BrC}(370)$, $\%Abs_{BrC}$ and AAE overall increased by 0.43 %/year, 1.91 %/year, 0.64 %/year, respectively. The meta analysis provided s.s. trends for $b_{Abs}(370)$, $b_{Abs,BC}(370)$, AAE and $\%Abs_{BrC}$, indicating homogeneity of the trends for these variables in Europe, whereas overall the trends were not s.s. for $b_{Abs,BrC}(370)$ and AAE_{BrC} indicating more heterogeneity of the trend results. Among all the station backgrounds reported in Fig. 7, traffic sites were those

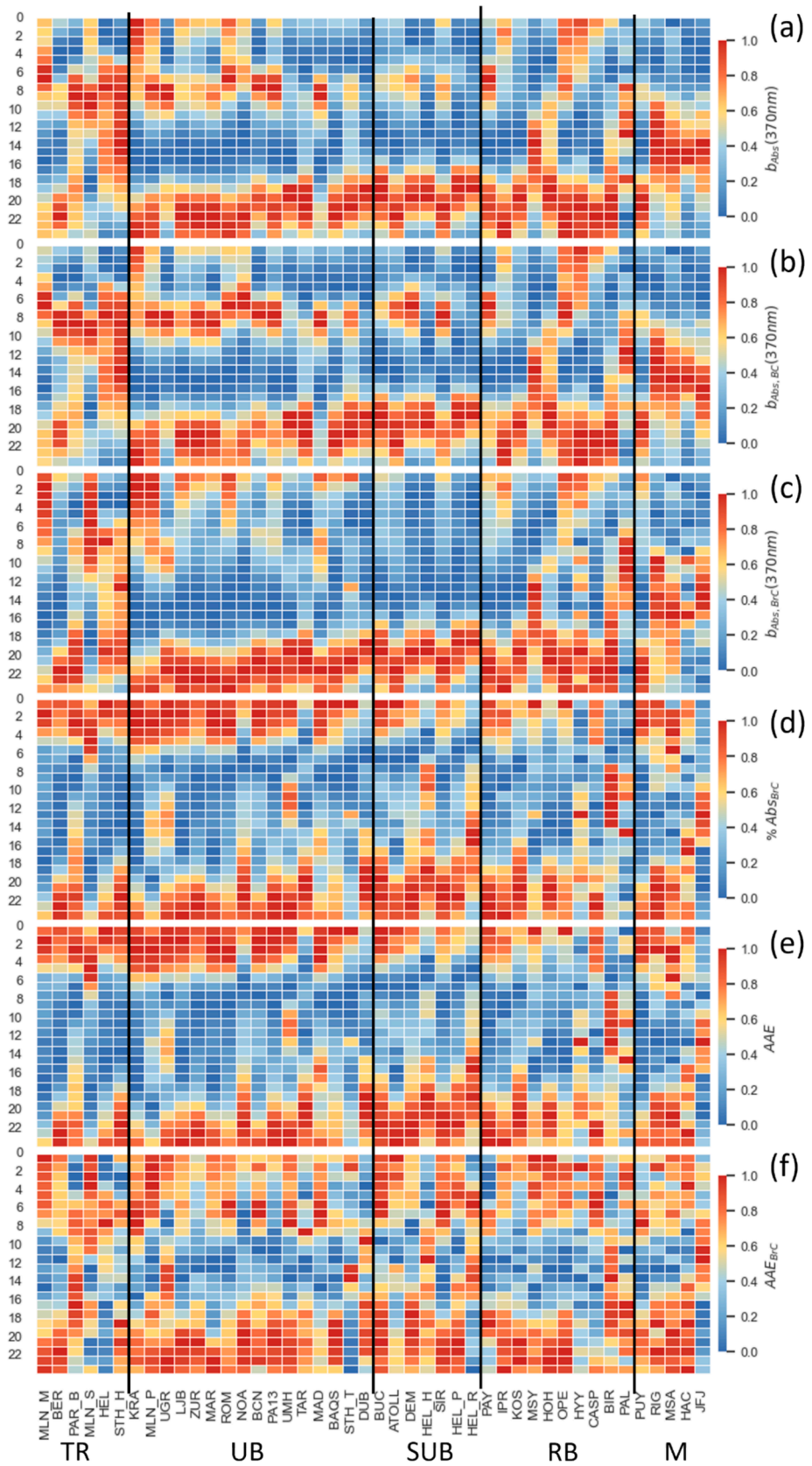

Fig. 6. Normalized diel cycles of the same variables as in Fig. 5.

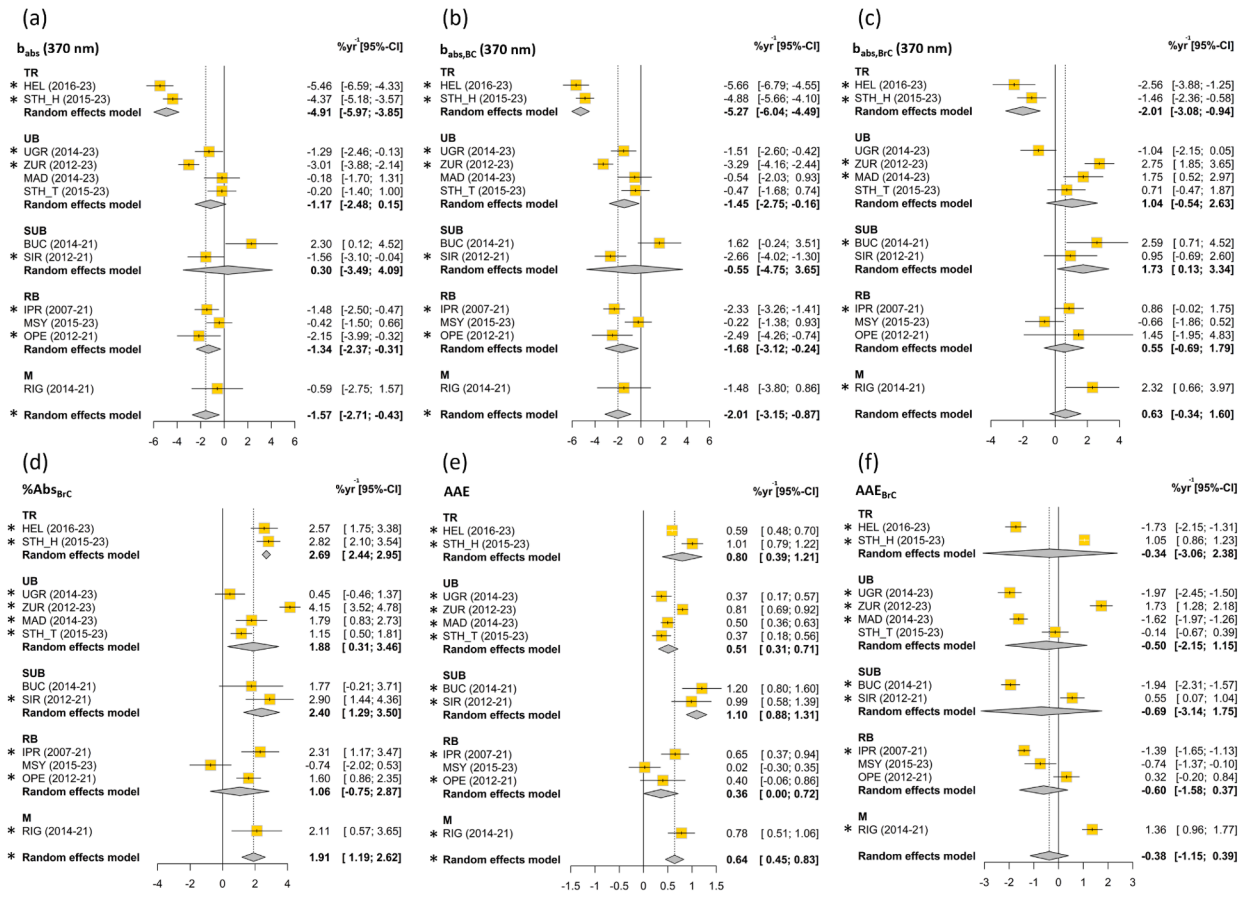

Fig. 7. Results of the trend analysis and subsequent *meta*-analysis for $b_{Abs}(370)$ (a), $b_{Abs,BC}(370)$ and $b_{Abs,BrC}(370)$ (b and c, respectively), relative contribution of $b_{Abs,BrC}(370)$ to $b_{Abs}(370)$ (d), AAE of CA from 370 to 950 nm (e), and AAE of BrC from 370 to 660 (f). Trends are calculated using the Mann-Kendall non-parametric method. * indicates statistically significant trends ($p < 0.01$). Results of the *meta*-analysis are presented globally for each variable and for the different site categories (TR, UB, SUB, RB and M). The dashed vertical line represents the global *meta*-analysis. Random effects model: mean effect calculated for each site typology and for all sites together.

characterized by the strongest magnitude of decreasing trends for $b_{Abs}(370)$ (−4.4 to −5.5 %/year) and $b_{Abs,BC}(370)$ (−4.9 to −5.7 %/year), thus confirming the effective reduction of BC emissions from traffic sources. These trends demonstrated the efficient reduction of BC mass concentrations from traffic sources in Europe suggesting a positive impact of the implementation of EURO 5/V and 6/VI vehicle standards (e.g. Kutzner et al., 2018; Sun et al., 2021; Savadkoohi et al., 2023; Garcia-Marlès et al., 2024) and a less effective reduction of emissions from BrC sources, likely mostly from domestic biomass burning (e.g. Yttri et al., 2021; Savadkoohi et al., 2023). For example, Savadkoohi et al. (2023) have reported statistically significant decreasing trends for BC from traffic sources in Europe whereas BC from domestic sources remained constant or even increased slightly in some European cities. At UB, SUB and RB sites, the magnitude of the s.s. decreasing trends for $b_{Abs}(370)$ (−1.3 to −3.0 %/year) and $b_{Abs,BC}(370)$ (−1.5 to −3.3 %/year) were lower suggesting the presence of regional contributions of BC to absorption. These regional sources of BC, mostly biomass burning, also contributed to explain the observed s.s. increasing trends of AAE and % Abs_{BrC}.

The observed increase of AAE calculated from 370 to 950 nm confirmed a progressive change in the chemical composition of CA particles driven by a relative increase/decrease of BrC/BC content in CA with time. Recently, Yttri et al. (2021) reported large decreases in EC and a relatively smaller decline in levoglucosan at the BIR measurement site in northern Europe, suggesting that the OC and EC from traffic and industry were decreasing, whereas the abatement of OC and EC from biomass burning was less successful. Similarly, in 't Veld et al. (2021) reported for both BCN and MSY (NE Spain) the absence of a trend for OM driven by secondary organic aerosols formation, whereas EC showed s.s. decreasing trends at both sites. The s.s. decreasing trends observed here for $b_{Abs,BC}(370)$ agreed also with the results from the recent study by Aas et al. (2024) reporting decreasing trends for elemental carbon (EC) mass concentrations in Europe during 2010–2019. These EC decreasing trends were mostly associated with reduced vehicular emissions, as also reported for the decreasing trends of BC in Europe by Savadkoohi et al. (2023). Aas et al. (2024) also reported decreasing trends for OC mass concentrations even in smaller magnitude and significance compared to EC. Indeed, the OC decreasing trends reported by Aas et al. (2024) were s.s. only at 2 out of 15 sites included in their work and the highest magnitude and statistically significance of the OC trends were observed in winter consistent with the reduction of primary organic aerosols from EC sources. It is not straightforward to correlate the $b_{Abs,BrC}(370)$ trends reported here with the OC trends reported in Aas et al. (2024) as the different time granularity, data coverage and measuring periods can affect the trend analysis especially over short periods. The $b_{Abs,BrC}(370)$ showed s.s. increasing trends at 5 out of 10 non-traffic sites and, as aforementioned, the overall increasing trend in Europe for $b_{Abs,BrC}(370)$ was non s.s. due to the heterogeneity of the trends among the 12 sites. The trend results for $b_{Abs,BrC}(370)$ at non-traffic sites suggested multiple origins of BC and BrC (mostly traffic and biomass burning) and reflected the slower and less significant decreasing trends observed for OC in Europe compared to EC. Among the sites used here for $b_{Abs,BrC}(370)$ trend analysis, four sites (IPR, MSY, OPE and RIG) were also included in the trend study from Aas et al. (2024) for OC. Aas et al. (2024) reported

s.s. OC decreasing trend (2010–2019) only for IPR where $b_{Abs,BrC}(370)$ showed s.s. increasing trend as in RIG. Thus, the s.s increasing trends of $b_{Abs,BrC}(370)$ observed here at some sites (5 out of 10 non-traffic sites) could suggest a shift toward organic matter particles with higher mass-specific absorption efficiency. This shift could be at least in part related to the observed increase of ammonia (NH_3) concentrations in Europe reported by Aas et al. (2024). In fact, chamber experiments have shown the increase of the absorption efficiency of a wide range of biogenic and anthropogenic secondary organic aerosols formed under high NH3 emissions (e.g. Updyke et al., 2012).

Interestingly, the $b_{Abs,BrC}(370)$ showed s.s. decreasing trends only at the two traffic sites included in this analysis (HEL and STH_H) thus suggesting traffic emissions as the main source of both BC and BrC at these sites. Despite the observed decrease of $b_{Abs,BC}(370)$ and $b_{Abs,BrC}(370)$ at the traffic stations, both $\%Abs_{BrC}$ and AAE increased. Beside the increase of the relative proportion of regional aerosols due to the decrease of BC emissions from local traffic, the observed $\%Abs_{BrC}$ and AAE increase suggested a more effective decrease of BC compared to BrC in CA particles from vehicles.

As already mentioned, the change of CA chemical composition with time observed in Europe had an important impact in the AAE, an intensive optical parameter that strongly depends on the chemical composition of particles. The effect of CA compositional changes on CA optical properties has been for example reported for the MSY site by Yus-Díez et al. (2022). Yus-Díez et al. (2022) showed that the absorption enhancement of BC particles increased at MSY station over the 2011–2020 period during spring and summer, when the OC/EC ratio, driven by secondary organic aerosol formation, increased along with the oxidation state of CA particles. Differently from the AAE, the AAE_{BrC} showed s.s. decreasing trends at 5 sites out of 12 and s.s. increasing trends at 4 sites without a clear relationship with station background. As mentioned above, it is not straightforward to understand the AAE_{BrC} variability without detailed OM chemical analysis and knowledge on the BC mixing state. Based, for example, on Saleh et al. (2013, 2014) and Kumar et al. (2018), a decreasing/increasing trend of AAE_{BrC} could suggest a progressive shift toward OM particles with more/less absorbing efficiency (i.e. higher/lower imaginary refractive index). Summarizing, the trend analyses reported here reflected the general change in CA composition and emission over time in Europe demonstrating a strong reduction of the absorption due to BC particles from traffic and a relative increase in the contribution of OM particles to total absorption.

4. Conclusions

This study provides a phenomenological analysis of total absorption at 370 nm ($b_{Abs}(370)$), BC and BrC contributions to absorption ($b_{Abs,BC}(370)$ and $b_{Abs,BrC}(370)$), absorption Ångström exponent (AAE) of both carbonaceous aerosol (CA) and brown carbon (BrC) particles (AAE_{BrC}) using Aethalometer data collected at 44 European sites.

A considerable variation of the absorption coefficients among the measurement sites was observed. This variation was influenced mostly by station background and showed a clear increase from mountain to urban and traffic sites. Mountain site absorption was influenced by altitude, topographical factors and atmospheric boundary layer influence. High site-by-site variability was exhibited at regional, urban and traffic stations related to location, proximity to CA emission sources, local meteorology, and variability in CA sources. Some hotspots (e.g. Krakow, Milan, Ispra and Paris) displayed particularly high absorption levels due to high local pollution and atmospheric conditions.

Similarly to $b_{Abs}(370)$, both $b_{Abs,BC}(370)$ and $b_{Abs,BrC}(370)$ increased from mountain to urban and traffic sites with notable site-by-site variability, attributed to POA particles, fuel type used, combustion conditions, and the influence of SOA. Apart from traffic sites, with lower relative contribution of BrC PM to $b_{Abs}(370)$ ($\%Abs_{BrC}$ median 11–20 %), the station setting was not the main parameter determining the reported $\%Abs_{BrC,}$ being the intensity of POA emissions and SOA formation the likely main factors driving the variability of $\%Abs_{BrC}$ and AAE. At all sites the AAE_{BrC} was considerably higher than AAE as a consequence of the stronger wavelength dependence of BrC PM, strengthening the argument that the SOA contribution to absorption is an important factor determining the wavelength dependence of BrC absorption. Further analyses are needed to better understand the variability of AAE_{BrC} which was influenced by the physico-chemical properties and transformation processes of BrC PM, particularly by their absorption characteristics in different spectral ranges.

All the variables reported here, with the exception of AAE_{BrC}, showed relative maxima in winter suggesting higher CA emissions from household activities and accumulation favored by predominant stagnant conditions and lower planetary boundary heights during the cold months. Conversely, relative minima were observed in summer due to higher wind speeds and atmospheric dispersion and to a reduction of BrC emissions. The diel cycles of $b_{Abs}(370)$ and $b_{Abs,BC}(370)$ showed bimodal peaks during morning and evening rush hours, with a midday decrease due to atmospheric dispersion and reduced emissions, except at mountain sites where both increased at noon, facilitated by higher mixing layers. In contrast, $b_{Abs,BrC}(370)$, $\%Abs_{BrC}$ and AAE peaked at night likely due increased domestic activities and nighttime formation of brown SOA. Traffic sites showed synchronized $b_{Abs,BC}(370)$ and $b_{Abs,BrC}(370)$ pattern, confirming vehicle emissions as a source of BrC PM. Notably, AAE_{BrC} showed diel cycles with lower values during the day and higher values at night and early morning, suggesting nighttime accumulation or formation of BrC PM with enhanced absorption efficiency in UV compared to the visible spectrum as could be expected for brown SOA.

Finally, this study conducted trend analysis at 12 monitoring sites, with at least 8 years of data availability, showing s.s. decreasing trends in $b_{Abs}(370)$ primarily driven by declining $b_{Abs,BC}(370)$. The observed s.s. increasing trends of $\%Abs_{BrC}$, confirmed recent evidence that the OC and BC concentrations from traffic and industry were efficiently decreasing in Europe, whereas the abatement of OC and BC from biomass burning has been slightly less successful. Indeed, only the traffic sites showed s.s. decreasing trends in both $b_{Abs,BrC}(370)$ and $b_{Abs,BC}(370)$, suggesting, as aforementioned, traffic emissions as the main source of both BC and BrC at traffic sites. As a consequence, the trend analyses revealed a progressive change in CA chemical composition with s.s. increasing trends in AAE driven by a relative increase/decrease of BrC/BC content in CA particles. The fact that $\%Abs_{BrC}$ generally increased across sites, suggests open challenges in reducing BrC emissions effectively.

This study, based on pan-european data confirms the effective reduction of BC emissions from vehicles thanks to the implementation of EURO 5/V and 6/VI vehicle standards and a less effective reduction of BC and BrC emissions from sources as household activities. The results presented in this work also align with the new European Air Quality Directive adopted on 14th October 2024 that establishes that black carbon, together with other emerging pollutants such as ultrafine particles, should be measured at monitoring supersites at both rural and urban background locations in order to support scientific understanding of its effects on human health and the environment. Furthermore, the observed general increasing trends of the contribution of BrC PM to absorption reported here support recent assessments (e.g. Zauli-Sajani et al., 2024) that indicate that the residential sector should be a key target of air quality policies and that promoting biomass as a carbon–neutral energy source could have a detrimental effect on both air quality and climate.

CRediT authorship contribution statement

Jordi Rovira: Writing – review & editing, Writing – original draft, Visualization, Investigation, Formal analysis, Data curation. **Marjan**

Savadkoohi: Writing – review & editing, Visualization, Formal analysis, Data curation. **Gang I. Chen:** Writing – review & editing, Data curation. **Griša Močnik:** Writing – review & editing, Methodology. **Wenche Aas:** Writing – review & editing, Data curation. **Lucas Alados-Arboledas:** Funding acquisition, Data curation. **Begoña Artiñano:** Funding acquisition, Data curation. **Minna Aurela:** Data curation. **John Backman:** Writing – review & editing, Data curation. **Sujai Banerji:** Data curation. **David Beddow:** Data curation. **Benjamin Brem:** Data curation. **Benjamin Chazeau:** Data curation. **Martine Collaud Coen:** Writing – review & editing, Data curation. **Cristina Colombi:** Writing – review & editing, Data curation. **Sebastien Conil:** Data curation. **Francesca Costabile:** Writing – review & editing, Funding acquisition, Data curation. **Esther Coz:** Data curation. **Joel F. de Brito:** Writing – review & editing, Funding acquisition, Data curation. **Kostas Eleftheriadis:** Writing – review & editing, Funding acquisition, Data curation. **Olivier Favez:** Funding acquisition, Data curation. **Harald Flentje:** Data curation. **Evelyn Freney:** Data curation. **Asta Gregorič:** Data curation. **Martin Gysel-Beer:** Writing – review & editing, Funding acquisition, Data curation. **Roy Harrison:** Writing – review & editing, Data curation. **Christoph Hueglin:** Data curation. **Antti Hyvärinen:** Data curation. **Matic Ivančič:** Writing – review & editing, Data curation. **Athina-Cerise Kalogridis:** Data curation. **Hannes Keernik:** Data curation. **Granakis Konstantinos:** Data curation. **Paolo Laj:** Data curation. **Eleni Liakakou:** Writing – review & editing, Data curation. **Chunshui Lin:** Data curation. **Stefano Listrani:** Data curation. **Krista Luoma:** Data curation. **Marek Maasikmets:** Data curation. **Hanna E. Manninen:** Data curation. **Nicolas Marchand:** Funding acquisition, Data curation. **Sebastiao Martins dos Santos:** Data curation. **Saliou Mbengue:** Writing – review & editing, Data curation. **Nikos Mihalopoulos:** Writing – review & editing, Data curation. **Doina Nicolae:** Data curation. **Jarkko V. Niemi:** Writing – review & editing, Data curation. **Michael Norman:** Writing – review & editing, Data curation. **Jurgita Ovadnevaite:** Writing – review & editing, Data curation. **Jean-Eudes Petit:** Data curation. **Stephen Platt:** Writing – review & editing, Data curation. **André S.H. Prévôt:** Writing – review & editing, Funding acquisition, Data curation. **Manuel Pujadas:** Data curation. **Jean-Philippe Putaud:** Funding acquisition, Data curation. **Véronique Riffault:** Writing – review & editing, Data curation. **Martin Rigler:** Writing – review & editing, Funding acquisition, Data curation. **Matteo Rinaldi:** Funding acquisition, Data curation. **Jaroslav Schwarz:** Data curation. **Sanna Silvergren:** Writing – review & editing, Funding acquisition, Data curation. **Erik Teinemaa:** Data curation. **Kimmo Teinilä:** Data curation. **Hilkka Timonen:** Writing – review & editing, Data curation. **Gloria Titos:** Writing – review & editing, Funding acquisition, Data curation. **Anna Tobler:** Data curation. **Jeni Vasilescu:** Writing – review & editing, Funding acquisition, Data curation. **Stergios Vratolis:** Writing – review & editing, Data curation. **Karl Espen Yttri:** Writing – review & editing, Data curation. **Eduardo Yubero:** Writing – review & editing, Funding acquisition, Data curation. **Naděžda Zíková:** Data curation. **Andrés Alastuey:** Writing – review & editing, Funding acquisition, Data curation. **Tuukka Petäjä:** Funding acquisition, Data curation. **Xavier Querol:** Writing – review & editing, Funding acquisition, Data curation. **Jesús Yus-Díez:** Writing – review & editing, Validation, Methodology, Conceptualization. **Marco Pandolfi:** Writing – review & editing, Validation, Supervision, Resources, Methodology, Funding acquisition, Conceptualization.

Declaration of competing interest

The authors declare that they have no known competing financial interests or personal relationships that could have appeared to influence the work reported in this paper. Griša Močnik, Asta Gregorič, Matic Ivančič and Martin Rigler were or are employed by the manufacturer of the instruments used in this study.

Acknowledgments

This study was supported by the EU HORIZON-EUROPE project FOCI under grant agreement n° 101056783, by the RI-URBANS project (Research Infrastructures Services Reinforcing Air Quality Monitoring Capacities in European Urban & Industrial Areas, European Union's Horizon 2020 research and innovation program, Green Deal, European Commission, contract 101036245), by the "Agencia Estatal de Investigación " from the Spanish Ministry of Science and Innovation, the Generalitat de Catalunya (AGAUR 2021 SGR 00447), the project CAIAC (PID2019-108990RB-I00) and FPI grant (PRE-2020-095498), by Generalitat de Catalunya (D.G. Atmospheric Pollution Prevention and Control, and AGAUR 2017 SGR41), by the Agencia Estatal de Investigación from the Spanish Ministry of Science and Innovation, FEDER funds under the projects AIRPHONEMA (PID2022-142160OB-I00). We would like to thank ACTRIS for providing Aethalometer absorption data for some sites of this study, and National and City authorities for providing others. Griša Močnik and Asta Gregorič gratefully acknowledge partial funding by ARIS program P1-0385. Irish datasets were supported by the EPA-Ireland (AEROSOURCE), the Department of Environment, Climate and Communications. Supported by the Core Program within the Romanian National Research Development and Innovation Plan 2022-2027, carried out with the support of MCID, project no. PN 23 05. Multi-wavelength absorption data for Birkenes Observatory is obtained as part of the Norwegian national monitoring programme (Platt et al., 2023) and is funded by the Norwegian Environment Agency (Contract No. 21087006). The continuous aerosol measurements at the Jungfraujoch (JFJ) site are supported by MeteoSwiss in the framework of the Swiss contributions (GAW-CH) to the Global Atmosphere Watch program of the World Meteorological Organization (WMO) and ACTRIS Switzerland funded by the Swiss State Secretariat for Education, Research and Innovation (SERI), also the International Foundation High Altitude Research Stations Jungfraujoch and Gornergrat (HFSJG) is acknowledged for support. ATOLL measurements have been supported by the Labex CaPPA project, which is funded by the French National Research Agency (ANR) through the PIA (Programme d'Investissement d'Avenir) under contract ANR-11-LABX-0005-01; the CLIMIBIO and ECRIN projects, all financed by the Regional Council "Hauts-de-France" and the European Regional Development Fund (ERDF); the COST COLOSSAL Action (CA16109); and the French Ministry of Environment through the CARA program of the Laboratoire Central de Surveillance de la Qualité de l'Air (LCSQA). Long-term continuous aerosol measurements at Granada (UGR) site are supported by NUCLEUS (PID2021-128757OB-I00) funded by MICIU/AEI/10.13039/501100011033 and by ERDF A way of making Europe, ACTRIS-España (RED2022-134824-E), and by University of Granada Plan Propio through Excellence Research Unit Earth Science and Singular Laboratory AGORA (LS2022-1) programs. Long-term continuous aerosol light absorption measurements at Rome (ROM) site are supported by the Latium Environmental Protection Agency (ARPA Lazio), and the support of Alessandro Di Giosa and Stefano Listrani is gratefully acknowledged. Finnish Meteorological gratefully acknowledges funding from Academy of Finland via the project Black and Brown Carbon in the Atmosphere and the Cryosphere (BBrCAC) (decision nr. 341271). Jesús Yus-Díez is supported by the European Union's Horizon Europe research and innovation programme under the Marie Skłodowska-Curie Postdoctoral Fellowship Programme, SMASH is co-funded by the Republic of Slovenia and the European Union from the European Regional Development Fund under the grant agreement No. 101081355.

Appendix A. Supplementary data

Supplementary data to this article can be found online at https://doi.org/10.1016/j.envint.2024.109185.

Data availability

Data will be made available on https://doi.org/10.5281/zenodo.13365276.

References

Aas, W., Fagerli, H., Alastuey, A., Cavalli, F., Degorska, A., Feigenspan, S., Brenna, H., Gliß, J., Heinesen, D., Hueglin, C., Holubová, A., Jaffrezo, J.-L., Mortier, A., Murovec, M., Putaud, J.-P., Rüdige, J., Simpson, D., Solberg, S., Tsyro, S., Tørseth, K., 2024. Trends in Air Pollution in Europe, 2000–2019. Aerosol Air Qual. Res. 24, 230237. https://doi.org/10.4209/aaqr.230237.

Alastuey, A., Querol, X., Aas, W., Lucarelli, F., Pérez, N., Moreno, T., Cavalli, F., Areskoug, H., Balan, V., Catrambone, M., Ceburnis, D., Cerro, J.C., Conil, S., Gevorgyan, L., Hueglin, C., Imre, K., Jaffrezo, J.-L., Leeson, S.R., Mihalopoulos, N., Mitosinkova, M., 2016. Geochemistry of PM10 over Europe during the EMEP intensive measurement periods in summer 2012 and winter 2013. Atmos. Chem. Phys. 16, 6107–6129. https://doi.org/10.5194/acp-16-6107-2016.

Balduzzi, S., Rücker, G., Schwarzer, G., 2019. How to perform a meta-analysis with R: a practical tutorial. Evidence Based Mental Health 22, 153–160. https://doi.org/10.1136/ebmental-2019-300117.

Barreira, L.M.F., Helin, A., Aurela, M., Teinilä, K., Friman, M., Kangas, L., Niemi, J.V., Portin, H., Kousa, A., Pirjola, L., Rönkkö, T., Saarikoski, S., Timonen, H., 2021. In-depth characterization of submicron particulate matter inter-annual variations at a street canyon site in northern Europe. Atmos. Chem. Phys. 21, 6297–6314. https://doi.org/10.5194/acp-21-6297-2021.

Bigi, A., Vogt, F.P.A., 2021. mannkendall/R: Bug fix: prob_mk_n, Version v1.1.0. Zenodo. https://doi.org/10.5281/zenodo.4495588.

Blanco-Alegre, C., Calvo, A.I., Alves, C., Fialho, P., Nunes, T., Gomes, J., Castro, A., Oduber, F., Coz, E., Fraile, R., 2020. Aethalometer measurements in a road tunnel: A step forward in the characterization of black carbon emissions from traffic. Sci. Total Environ. 703, 135483. https://doi.org/10.1016/j.scitotenv.2019.135483.

Bond, T.C., Bergstrom, R.W., 2006. Light absorption by carbonaceous particles: an investigative review. Aerosol. Sci. Technol. 40, 27–67. https://doi.org/10.1080/02786820500421521.

Bond, T.C., Doherty, S.J., Fahey, D.W., Forster, P.M., Berntsen, T., DeAngelo, B.J., Flanner, M.G., Ghan, S., Kärcher, B., Koch, D., Kinne, S., Kondo, Y., Quinn, P.K., Sarofim, M.C., Schultz, M.G., Schulz, M., Venkataraman, C., Zhang, H., Zhang, S., Bellouin, N., Guttikunda, S.K., Hopke, P.K., Jacobson, M.Z., Kaiser, J.W., Klimont, Z., Lohmann, U., Schwarz, J.P., Shindell, D., Storelvmo, T., Warren, S.G., Zender, C.S., 2013. Bounding the role of black carbon in the climate system: A scientific assessment. J. Geophys. Res.-Atmos. 118, 5380–5552. https://doi.org/10.1002/jgrd.50171.

Brown, H., Liu, X., Feng, Y., Jiang, Y., Wu, M., Lu, Z., Wu, C., Murphy, S., Pokhrel, R., 2018. Radiative effect and climate impacts of brown carbon with the Community Atmosphere Model (CAM5). Atmos. Chem. Phys. 18, 17745–17768. https://doi.org/10.5194/acp-18-17745-2018.

Bukowiecki, N., Weingartner, E., Gysel, M., Collaud Coen, M., Zieger, P., Herrmann, E., Steinbacher, M., Gäggeler, H.W., Baltensperger, U., 2016. A review of more than 20 years of aerosol observation at the high altitude research station Jungfraujoch. Switzerland (3580 m asl) 16, 764–788. https://doi.org/10.4209/aaqr.2015.05.0305.

Casotto, R., Skiba, A., Rauber, M., Strähl, J., Tobler, A., Bhattu, D., Lamkaddam, H., Manousakas, M.I., Salazar, G., Cui, T., Canonaco, F., Samek, L., Ryś, A., El Haddad, I., Kasper-Giebl, A., Baltensperger, U., Necki, J., Szidat, S., Styszko, K., Slowik, J.G., 2023. Organic aerosol sources in Krakow, Poland, before implementation of a solid fuel residential heating ban. Sci. Total Environ. 855, 158655. https://doi.org/10.1016/j.scitotenv.2022.158655.

Casquero-Vera, J.A., Lyamani, H., Titos, G., Minguillón, M.C., Dada, L., Alastuey, A., Querol, X., Petäjä, T., Olmo, F.J., Alados-Arboledas, L., 2021. Quantifying traffic, biomass burning and secondary source contributions to atmospheric particle number concentrations at urban and suburban sites. Sci. Total Environ. 768, 145282. https://doi.org/10.1016/j.scitotenv.2021.145282.

Chakrabarty, R.K., Gyawali, M., Yatavelli, R.L.N., Pandey, A., Watts, A.C., Knue, J., Chen, L.-W.-A., Pattison, R.R., Tsibart, A., Samburova, V., Moosmüller, H., 2016. Brown carbon aerosols from burning of boreal peatlands: microphysical properties, emission factors, and implications for direct radiative forcing. Atmos. Chem. Phys. 16, 3033–3040. https://doi.org/10.5194/acp-16-3033-2016.

Chen, G., Canonaco, F., Tobler, A., Aas, W., Alastuey, A., Allan, J., Atabakhsh, S., Aurela, M., Baltensperger, U., Bougiatioti, A., De Brito, J.F., Ceburnis, D., Chazeau, B., Chebaicheb, H., Daellenbach, K.R., Ehn, M., El Haddad, I., Eleftheriadis, K., Favez, O., Flentje, H., 2022. European aerosol phenomenology – 8: Harmonised source apportionment of organic aerosol using 22 Year-long ACSM/AMS datasets. Environ. Int. 166, 107325. https://doi.org/10.1016/j.envint.2022.107325.

Chen, Y., Xie, X., Shi, Z., Li, Y., Gai, X., Wang, J., Li, H., Wu, Y., Zhao, X., Chen, M., Ge, X., 2020. Brown carbon in atmospheric fine particles in Yangzhou, China: Light absorption properties and source apportionment. Atmos. Res. 244, 105028. https://doi.org/10.1016/j.atmosres.2020.105028.

Collaud Coen, M., Weingartner, E., Schaub, D., Hueglin, C., Corrigan, C., Henning, S., Schwikowski, M., Baltensperger, U., 2004. Saharan dust events at the Jungfraujoch: detection by wavelength dependence of the single scattering albedo and first climatology analysis. Atmos. Chem. Phys. 4, 2465–2480. https://doi.org/10.5194/acp-4-2465-2004.

Collaud Coen, M., Weingartner, E., Apituley, A., Ceburnis, D., Fierz-Schmidhauser, R., Flentje, H., Henzing, B., Jennings, S.G., Moerman, M., Petzold, A., Schmid, O., Baltensperger, U., 2010. Minimizing light absorption measurement artifacts of the Aethalometer: evaluation of five correction algorithms. Atmos. Meas. Tech. 3, 457–474. https://doi.org/10.5194/amt-3-457-2010.

Collaud Coen, M., Andrews, E., Aliaga, D., Andrade, M., Angelov, H., Bukowiecki, N., Ealo, M., Fialho, P., Flentje, H., Hallar, A.G., Hooda, R., Kalapov, I., Krejci, R., Lin, N. H., Marinoni, A., Ming, J., Nguyen, N.A., Pandolfi, M., Pont, V., Ries, L., 2018. Identification of topographic features influencing aerosol observations at high altitude stations. Atmos. Chem. Phys. 18, 12289–12313. https://doi.org/10.5194/acp-18-12289-2018.

Collaud Coen, M., Andrews, E., Bigi, A., Martucci, G., Romanens, G., Vogt, F.P.A., Vuilleumier, L., 2020. Effects of the prewhitening method, the time granularity, and the time segmentation on the Mann–Kendall trend detection and the associated Sen's slope. Atmos. Meas. Tech. 13, 6945–6964. https://doi.org/10.5194/amt-13-6945-2020.

Corbin, J.C., Pieber, S.M., Czech, H., Zanatta, M., Jakobi, G., Massabò, D., Orasche, J., El Haddad, I., Mensah, A., Stengel, B., Drinovec, L., Močnik, G., Zimmermann, R., Prévôt, A.S.H., Gysel, M., 2018. Brown and black carbon emitted by a marine engine operated on heavy fuel oil and distillate fuels: optical properties. Size Distributions, and Emission Factors 123, 6175–6195. https://doi.org/10.1029/2017jd027818.

Cordell, R., Mazet, M., Dechoux, C., Hama, S., Staelens, J., Hofman, J., Stroobants, C., Roekens, E., Kos, G.P.A., Weijers, E.P., Frumau, K.F.A., Panteliadis, P., Delaunay, T., Wyche, K., Monks, P.S., 2016. Evaluation of biomass burning across North West Europe and its impact on air quality. Atmos. Environ. 141, 276–286. https://doi.org/10.1016/j.atmosenv.2016.06.065.

Costabile, F., Gilardoni, S., Barnaba, F., Di Ianni, A., Di Liberto, L., Dionisi, D., Manigrasso, M., Paglione, M., Poluzzi, V., Rinaldi, M., Facchini, M.C., Gobbi, G.P., 2017. Characteristics of brown carbon in the urban Po Valley atmosphere. Atmos. Chem. Phys. 17, 313–326. https://doi.org/10.5194/acp-17-313-2017.

Cuesta-Mosquera, A., Močnik, G., Drinovec, L., Müller, T., Pfeifer, S., Minguillón, M.C., Briel, B., Buckley, P., Dudoitis, V., Fernández-García, J., Fernández-Amado, M., Ferreira, J., Riffault, V., Flentje, H., Heffernan, E., Kalivitis, N., Kalogridis, A.-C., Keernik, H., Marmureanu, L., Luoma, K., 2021. Intercomparison and characterization of 23 Aethalometers under laboratory and ambient air conditions: procedures and unit-to-unit variabilities. Atmos. Meas. Tech. 14, 3195–3216. https://doi.org/10.5194/amt-14-3195-2021.

Cuesta-Mosquera, A., Glojek, K., Močnik, G., Drinovec, L., Gregorič, A., Rigler, M., Ogrin, M., Romshoo, B., Weinhold, K., Merkel, M., van Pinxteren, D., Herrmann, H., Wiedensohler, A., Pöhlker, M., Müller, T., 2024. Optical properties and simple forcing efficiency of the organic aerosols and black carbon emitted by residential wood burning in rural central Europe. Atmos. Chem. Phys. 24, 2583–2605. https://doi.org/10.5194/acp-24-2583-2024.

Dong, Z., Pavuluri, C.M., Li, P., Xu, Z., Deng, J., Zhao, X., Zhao, X., Fu, P., Liu, C.-Q., 2024. Measurement report: Optical characterization, seasonality, and sources of brown carbon in fine aerosols from Tianjin, North China: year-round observations. Atmos. Chem. Phys. 24, 5887–5905. https://doi.org/10.5194/acp-24-5887-2024.

Drinovec, L., Močnik, G., Zotter, P., Prévôt, A.S.H., Ruckstuhl, C., Coz, E., Rupakheti, M., Sciare, J., Müller, T., Wiedensohler, A., Hansen, A.D.A., 2015. The "dual-spot" Aethalometer: an improved measurement of aerosol black carbon with real-time loading compensation. Atmos. Meas. Tech. 8, 1965–1979. https://doi.org/10.5194/amt-8-1965-2015.

Ealo, M., Alastuey, A., Ripoll, A., Pérez, N., Minguillón, M.C., Querol, X., Pandolfi, M., 2016. Detection of Saharan dust and biomass burning events using near-real-time intensive aerosol optical properties in the north-western Mediterranean. Atmos. Chem. Phys. 16, 12567–12586. https://doi.org/10.5194/acp-16-12567-2016.

EC, 2011. Commission Staff Working Paper Establishing Guidelines for Determination of Contributions From the Re-suspension of Particulates Following Winter Sanding or Salting of Roads Under the Directive 2008/50/EC on Ambient Air Quality and Cleaner Air for Europe. vol. 207. European Commission,SEC 2011. 43pp. http://ec.europa.eu/environment/air/quality/legislation/pdf/sec_2011_0207.pdf.

Fang, W., Andersson, A., Lee, M., Zheng, M., Du, K., Kim, S.-W., Holmstrand, H., Gustafsson, Ö., 2023. Combined influences of sources and atmospheric bleaching on light absorption of water-soluble brown carbon aerosols. In: Npj Climate and Atmospheric Science 6. https://doi.org/10.1038/s41612-023-00438-8.

Feng, Y., Ramanathan, V., Kotamarthi, V.R., 2013. Brown carbon: a significant atmospheric absorber of solar radiation? Atmos. Chem. Phys. 13, 8607–8621. https://doi.org/10.5194/acp-13-8607-2013.

Ferrero, L., Močnik, G., Cogliati, S., Gregorič, A., Colombo, R., Bolzacchini, E., 2018. Heating rate of light absorbing aerosols: time-resolved measurements, the role of clouds, and source identification. Environ. Sci. Tech. 52, 3546–3555. https://doi.org/10.1021/acs.est.7b04320.

Ferrero, L., Gregorič, A., Močnik, G., Rigler, M., Cogliati, S., Barnaba, F., Di Liberto, L., Gobbi, G.P., Losi, N., Bolzacchini, E., 2021. The impact of cloudiness and cloud type on the atmospheric heating rate of black and brown carbon in the Po Valley. Atmos. Chem. Phys. 21, 4869–4897. https://doi.org/10.5194/acp-21-4869-2021.

Fleming, L.T., Lin, P., Roberts, J.M., Selimovic, V., Yokelson, R., Laskin, J., Laskin, A., Nizkorodov, S.A., 2020. Molecular composition and photochemical lifetimes of brown carbon chromophores in biomass burning organic aerosol. Atmos. Chem. Phys. 20, 1105–1129. https://doi.org/10.5194/acp-20-1105-2020.

Frka, S., Šala, M., Brodnik, H., Štefane, B., Kroflič, A., Grgić, I., 2022. Seasonal variability of nitroaromatic compounds in ambient aerosols: Mass size distribution, possible sources and contribution to water-soluble brown carbon light absorption. Chemosphere 299, 134381. https://doi.org/10.1016/j.chemosphere.2022.134381.

Garcia-Marlès, M., Lara, R., Reche, C., Pérez, N., Tobías, A., Savadkoohi, M., Beddows, D., Salma, I., Vörösmarty, M., Weidinger, T., Hueglin, C.,

Mihalopoulos, N., Grivas, G., Kalkavouras, P., Ondráček, J., Zíková, N., Niemi, J.V., Manninen, H.E., Green, D.C., Tremper, A.H., 2024. Inter-annual trends of ultrafine particles in urban Europe. Environ. Int. 185, 108510. https://doi.org/10.1016/j.envint.2024.108510.

Gilardoni, S., Massoli, P., Marinoni, A., Mazzoleni, C., Freedman, A., Lonati, G., De Iuliis, S., Gianelle, V., 2020. Spatial and temporal variability of carbonaceous aerosol absorption in the Po valley. Aerosol Air Qual. Res. 20, 2624–2639. https://doi.org/10.4209/aaqr.2020.03.0085.

Gilbert, R.O., 1987. Statistical Methods for Environmental Pollution Monitoring [WWW Document]. www.osti.gov. URL https://www.osti.gov/biblio/7037501 (accessed 7.29.24).

Gundel, L.A., Dod, R.L., Rosen, H., Novakov, T., 1984. The relationship between optical attenuation and black carbon. Sci. Total Environ. 36, 197–202. https://doi.org/10.1016/00489697(84)90266-3.

Harmsen, M.J.H.M., van Dorst, P., van Vuuren, D.P., van den Berg, M., Van Dingenen, R., Klimont, Z., 2020. Co-benefits of black carbon mitigation for climate and air quality. Clim. Change 163, 1519–1538. https://doi.org/10.1007/s10584-020-02800-8.

Harrison, R.M., Beddows, D.C.S., Jones, A.M., Calvo, A., Alves, C., Pio, C., 2013. An evaluation of some issues regarding the use of aethalometers to measure woodsmoke concentrations. Atmos. Environ. 80, 540–548. https://doi.org/10.1016/j.atmosenv.2013.08.026.

Ho, C.S., Lv, Z., Peng, J., Zhang, J., Choe, T.-H., Zhang, Q., Du, Z., Mao, H., 2023. Optical properties of vehicular brown carbon emissions: Road tunnel and chassis dynamometer tests. Environ. Pollut. 320, 121037. https://doi.org/10.1016/j.envpol.2023.121037.

Hopstock, K.S., Klodt, A.L., Xie, Q., Alvarado, M.A., Laskin, A., Nizkorodov, S.A., 2023. Photolytic aging of organic aerosol from pyrolyzed urban materials. Environ. Sci.: Atmos. 3, 1272–1285. https://doi.org/10.1039/d3ea00078h.

Hu, Z., Kang, S., Li, C., Yan, F., Chen, P., Gao, S., Wang, Z., Zhang, Y., Sillanpaa, M., 2017. Light absorption of biomass burning and vehicle emission-sourced carbonaceous aerosols of the Tibetan Plateau. Environ. Sci. Pollut. Res. Int. 24, 15369–15378. https://doi.org/10.1007/s11356-017-9077-3.

in 't Veld, M., Alastuey, A., Pandolfi, M., Amato, F., Pérez, N., Reche, C., Via, M., Minguillón, M.C., Escudero, M., Querol, X., 2021. Compositional changes of PM2.5 in NE Spain during 2009–2018: A trend analysis of the chemical composition and source apportionment. Sci. Total Environ. 795, 148728. https://doi.org/10.1016/j.scitotenv.2021.148728.

IPCC, 2013. AR5 Climate Change 2013: The Physical Science Basis — IPCC [WWW Document]. Ipcc.ch. URL https://www.ipcc.ch/report/ar5/wg1/.

IPCC, Intergovernmental Panel on Climate Change, 2021. Climate Change 2021 - The Physical Science Basis - Summary for Policymakers, Climate Change 2021: The Physical Science Basis. doi: 10.1017/9781009157896.

Jimenez, J.L., Canagaratna, M.R., Donahue, N.M., Prevot, A.S.H., Zhang, Q., Kroll, J.H., DeCarlo, P.F., Allan, J.D., Coe, H., Ng, N.L., Aiken, A.C., Docherty, K.S., Ulbrich, I.M., Grieshop, A.P., Robinson, A.L., Duplissy, J., Smith, J.D., Wilson, K.R., Lanz, V.A., Hueglin, C., 2009. Evolution of organic aerosols in the atmosphere. Science (New York N.Y.) 326, 1525–1529. https://doi.org/10.1126/science.1180353.

Kalbermatter, D.M., Močnik, G., Drinovec, L., Visser, B., Röhrbein, J., Oscity, M., Weingartner, E., Hyvärinen, A.-P., Vasilatou, K., 2022. Comparing black-carbon- and aerosol-absorption-measuring instruments – a new system using lab-generated soot coated with controlled amounts of secondary organic matter. Atmos. Meas. Tech. 15, 561–572. https://doi.org/10.5194/amt-15-561-2022.

Kaskaoutis, D.G., Grivas, G., Stavroulas, I., Bougiatioti, A., Liakakou, E., Dumka, U.C., Gerasopoulos, E., Mihalopoulos, N., 2021. Apportionment of black and brown carbon spectral absorption sources in the urban environment of Athens, Greece, during winter. Sci. Total Environ. 801, 149739. https://doi.org/10.1016/j.scitotenv.2021.149739.

Kaskaoutis, D.G., Petrinoli, K., Grivas, G., Kalkavouras, P., Tsagkaraki, M., Tavernaraki, K., Papoutsidaki, K., Stavroulas, I., Paraskevopoulou, D., Bougiatioti, A., Liakakou, E., Rashki, A., Sotiropoulou, R.E.P., Tagaris, E., Gerasopoulos, E., Mihalopoulos, N., 2024. Impact of peri-urban forest fires on air quality and aerosol optical and chemical properties: The case of the August 2021 wildfires in Athens, Greece. Sci. Total Environ. 907, 168028. https://doi.org/10.1016/j.scitotenv.2023.168028.

Kasthuriarachchi, N.Y., Rivellini, L.-H., Adam, M.G., Lee, A.K.Y., 2020. Light absorbing properties of primary and secondary brown carbon in a tropical urban environment. Environ. Sci. Tech. 54, 10808–10819. https://doi.org/10.1021/acs.est.0c02414.

Kendall, M.G., 1975. Rank Correlation Methods, 4th Edition. Charles Griffin, London.

Kirchstetter, T.W., Novakov, T., Hobbs, P.V., 2004. Evidence that the spectral dependence of light absorption by aerosols is affected by organic carbon. J. Geophys. Res. 109, D21208. https://doi.org/10.1029/2004JD004999.

Kumar, J., Beeler, P., Sumlin, B.J., Chakrabarty, R.K., 2023. Aggregation-induced enhancements in aerosol absorption and scattering across the black-brown continuum. J. Quantitative Spectroscopy & Radiative Transfer/journal of Quantitative Spectroscopy & Radiative Transfer 310, 108729. https://doi.org/10.1016/j.jqsrt.2023.108729.

Kumar, N.K., Corbin, J.C., Bruns, E.A., Massabó, D., Slowik, J.G., Drinovec, L., Močnik, G., Prati, P., Vlachou, A., Baltensperger, U., Gysel, M., El-Haddad, I., Prévôt, A.S.H., 2018. Production of particulate brown carbon during atmospheric aging of residential wood-burning emissions. Atmos. Chem. Phys. 18, 17843–17861. https://doi.org/10.5194/acp-18-17843-2018.

Kutzner, R.D., von Schneidemesser, E., Kuik, F., Quedenau, J., Weatherhead, E.C., Schmale, J., 2018. Long-term monitoring of black carbon across Germany. Atmos. Environ. 185, 41–52. https://doi.org/10.1016/j.atmosenv.2018.04.039.

Lack, D.A., Langridge, J.M., 2013. On the attribution of black and brown carbon light absorption using the Ångström exponent. Atmos. Chem. Phys. 13, 10535–10543. https://doi.org/10.5194/acp-13-10535-2013.

Lambe, A.T., Cappa, C.D., Massoli, P., Onasch, T.B., Forestieri, S.D., Martin, A.T., Cummings, M.J., Croasdale, D.R., Brune, W.H., Worsnop, D.R., Davidovits, P., 2013. Relationship between oxidation level and optical properties of secondary organic aerosol. Environ. Sci. Tech. 47, 6349–6357. https://doi.org/10.1021/es401043j.

Laskin, A., Laskin, J., Nizkorodov, S.A., 2015. Chemistry of atmospheric brown carbon. Chem. Rev. 115, 4335–4382. https://doi.org/10.1021/cr5006167.

Li, Q., Liu, D., Jiang, X., Tian, P., Wu, Y., Li, S., Hu, K., Liu, Q., Huang, M., Li, R., Bi, K., Kong, S., Ding, D., Yu, C., 2023. Concurrent photochemical whitening and darkening of ambient brown carbon. Atmos. Chem. Phys. 23, 9439–9453. https://doi.org/10.5194/acp-23-9439-2023.

Li, Y., Miao, Y., Che, H., Liu, S., 2021. On the heavy aerosol pollution and its meteorological dependence in Shandong province, China. Atmos. Res. 256, 105572. https://doi.org/10.1016/j.atmosres.2021.105572.

Li, X., Sun, N., Jin, Q., Zhao, Z., Wang, L., Wang, Q., Gu, X., Li, Y., Liu, X., 2022. Light absorption properties of black and brown carbon in winter over the North China Plain: Impacts of regional biomass burning. Atmos. Environ. 278, 119100. https://doi.org/10.1016/j.atmosenv.2022.119100.

Liakakou, E., Stavroulas, I., Kaskaoutis, D.G., Grivas, G., Paraskevopoulou, D., Dumka, U.C., Tsagkaraki, M., Bougiatioti, A., Oikonomou, K., Sciare, J., Gerasopoulos, E., Mihalopoulos, N., 2020. Long-term variability, source apportionment and spectral properties of black carbon at an urban background site in Athens, Greece. Atmos. Environ 222, 117137. https://doi.org/10.1016/j.atmosenv.2019.117137.

Lin, C., Ceburnis, D., Vaishya, A., Trubetskaya, A., Tan, Y., Wang, T., Smith, W., Johnson, R., Xu, W., Monaghan, R.F.D., O'Dowd, C., Ovadnevaite, J., 2023. Air quality—climate forcing double whammy from domestic firelighters. npj climate and atmospheric science 6. doi: 10.1038/s41612-023-00427-x.

Liu, J., Lin, P., Laskin, A., Laskin, J., Kathmann, S.M., Wise, M., Caylor, R., Imholt, F., Selimovic, V., Shilling, J.E., 2016. Optical properties and aging of light-absorbing secondary organic aerosol. Atmos. Chem. Phys. 16, 12815–12827. https://doi.org/10.5194/acp-16-12815-2016.

López-Caravaca, A., Crespo, J., Galindo, N., Yubero, E., Clemente, A., Castañer, R., Nicolás, J.F., 2024. Characterization of water-soluble organic carbon absorption at an urban background site in the south-eastern Iberian Peninsula. Atmos. Environ. 324, 120435. https://doi.org/10.1016/j.atmosenv.2024.120435.

Lu, Z., Streets, D.G., Winijkul, E., Yan, F., Chen, Y., Bond, T.C., Feng, Y., Dubey, M.K., Liu, S., Pinto, J.P., Carmichael, G.R., 2015. Light absorption properties and radiative effects of primary organic aerosol emissions. Environ. Sci. Tech. 49, 4868–4877. https://doi.org/10.1021/acs.est.5b00211.

Lyamani, H., Olmo, F.J., Foyo, I., Alados-Arboledas, L., 2011. Black carbon aerosols over an urban area in south-eastern Spain: Changes detected after the 2008 economic crisis. Atmos. Environ. 45, 6423–6432. https://doi.org/10.1016/j.atmosenv.2011.07.063.

Mann, H.B., 1945. Nonparametric tests against trend. Econometrica 13, 245. https://doi.org/10.2307/1907187.

Massabò, D., Caponi, L., Bernardoni, V., Bove, M.C., Brotto, P., Calzolai, G., Cassola, F., Chiari, M., Fedi, M., Fermo, P., Giannoni, M., Lucarelli, F., Nava, S., Piazzalunga, A., Valli, G., Vecchi, R., Prati, P., 2015. Multi-wavelength optical determination of black and brown carbon in atmospheric aerosols. Atmos. Environ. 108, 1–12. https://doi.org/10.1016/j.atmosenv.2015.02.058.

Moise, T., Flores, J.M., Rudich, Y., 2015. Optical Properties of Secondary Organic Aerosols and Their Changes by Chemical Processes 115, 4400–4439. https://doi.org/10.1021/cr5005259.

Moosmüller, H., Chakrabarty, R.K., 2011. Technical Note: Simple analytical relationships between Ångström coefficients of aerosol extinction, scattering, absorption, and single scattering albedo. Atmos. Chem. Phys. 11, 10677–10680. https://doi.org/10.5194/acp-11-10677-2011.

Moschos, V., Kumar, N.K., Daellenbach, K.R., Baltensperger, U., Prévôt, A.S.H., El Haddad, I., 2018. Source apportionment of brown carbon absorption by coupling ultraviolet–visible spectroscopy with aerosol mass spectrometry. Environ. Sci. Technol. Lett. 5, 302–308. https://doi.org/10.1021/acs.estlett.8b00118.

Moschos, V., Gysel-Beer, M., Modini, R.L., Corbin, J.C., Massabò, D., Costa, C., Danelli, S.G., Vlachou, A., Daellenbach, K.R., Szidat, S., Prati, P., Prévôt, A.S.H., Baltensperger, U., El Haddad, I., 2021. Source-specific light absorption by carbonaceous components in the complex aerosol matrix from yearly filter-based measurements. Atmos. Chem. Phys. 21, 12809–12833. https://doi.org/10.5194/acp-21-12809-2021.

Müller, T., Fiebig, M., 2018. ACTRIS In Situ Aerosol: Guidelines for Manual QC of AE33 absorption photometer data. https://www.actris-ecac.eu/ (accessed 2.4.24).

Ni, H., Huang, R.-J., Pieber, S.M., Corbin, J.C., Stefenelli, G., Pospisilova, V., Klein, F., Gysel-Beer, M., Yang, L., Baltensperger, U., El Haddad, I., Slowik, J.G., Cao, J., Prévôt, A.S.H., Dusek, U., 2021. Brown carbon in primary and aged coal combustion emission. Environ. Sci. Tech. 55, 5701–5710. https://doi.org/10.1021/acs.est.0c08084.

Pandolfi, M., Querol, X., Alastuey, A., Jimenez, J.L., Jorba, O., Day, D., Ortega, A., Cubison, M.J., Comerón, A., Sicard, M., Mohr, C., Prévôt, A.S.H., Minguillón, M.C., Pey, J., Baldasano, J.M., Burkhart, J.F., Seco, R., Peñuelas, J., van Drooge, B.L., Artiñano, B., 2014a. Effects of sources and meteorology on particulate matter in the Western Mediterranean Basin: An overview of the DAURE campaign. J. Geophys. Res. Atmos. 119, 4978–5010. https://doi.org/10.1002/2013jd021079.

Pandolfi, M., Ripoll, A., Querol, X., Alastuey, A., 2014b. Climatology of aerosol optical properties and black carbon mass absorption cross section at a remote high-altitude site in the western Mediterranean Basin. Atmos. Chem. Phys. 14, 6443–6460. https://doi.org/10.5194/acp-14-6443-2014.

Pandolfi, M., Alados-Arboledas, L., Alastuey, A., Andrade, M., Angelov, C., Artiñano, B., Backman, J., Baltensperger, U., Bonasoni, P., Bukowiecki, N., Collaud Coen, M., Conil, S., Coz, E., Crenn, V., Dudoitis, V., Ealo, M., Eleftheriadis, K., Favez, O., Fetfatzis, P., Fiebig, M., 2018. A European aerosol phenomenology – 6: scattering properties of atmospheric aerosol particles from 28 ACTRIS sites. Atmos. Chem. Phys. 18, 7877–7911. https://doi.org/10.5194/acp-18-7877-2018.

Paraskevopoulou, D., Kaskaoutis, D.G., Grivas, G., Bikkina, S., Tsagkaraki, M., Vrettou, I. M., Tavernaraki, K., Papoutsidaki, K., Stavroulas, I., Liakakou, E., Bougiatioti, A., Oikonomou, K., Gerasopoulos, E., Mihalopoulos, N., 2022. Brown carbon absorption and radiative effects under intense residential wood burning conditions in Southeastern Europe: New insights into the abundance and absorptivity of methanol-soluble organic aerosols. Sci. Total Environ. 860, 160434. https://doi.org/10.1016/j.scitotenv.2022.160434.

Pauraite, J., Dudoitis, V., Byčenkienė, S., 2023. Assessment of carbonaceous aerosol properties across an urban environment during the cold season. Atmos. 14, 1054. https://doi.org/10.3390/atmos14071054.

Platt, S.M., Myhre, C.L., Svendby, T., Hermansen, O., Lunder, C., Fiebig, M., Fjæraa, A. M., Hansen, G., Schmidbauer, N., and Stebel, K. (2023). Monitoring of greenhouse gases and aerosols at Svalbard and Birkenes in 2022. Annual report. (NILU report 24/2023). Kjeller: NILU.

Putaud, J.-P., Cavalli, F., Crippa, M., 2018. Long-term trends in black carbon from biomass and fossil fuel combustion detected at the JRC atmospheric observatory in Ispra. doi: 10.2760/5944.

Putaud, J.-P., Raes, F., Van Dingenen, R., Brüggemann, E., Facchini, M.-C., Decesari, S., Fuzzi, S., Gehrig, R., Hüglin, C., Laj, P., Lorbeer, G., Maenhaut, W., Mihalopoulos, N., Müller, K., Querol, X., Rodriguez, S., Schneider, J., Spindler, G., ten Brink, H., Tørseth, K., 2004. A European aerosol phenomenology—2: chemical characteristics of particulate matter at kerbside, urban, rural and background sites in Europe. Atmos. Environ. 38, 2579–2595. https://doi.org/10.1016/j.atmosenv.2004.01.041.

Putaud, J.-P., Van Dingenen, R., Alastuey, A., Bauer, H., Birmili, W., Cyrys, J., Flentje, H., Fuzzi, S., Gehrig, R., Hansson, H.C., Harrison, R.M., Herrmann, H., Hitzenberger, R., Hüglin, C., Jones, A.M., Kasper-Giebl, A., Kiss, G., Kousa, A., Kuhlbusch, T.A.J., Löschau, G., 2010. A European aerosol phenomenology – 3: Physical and chemical characteristics of particulate matter from 60 rural, urban, and kerbside sites across Europe. Atmos. Environ. 44, 1308–1320. https://doi.org/10.1016/j.atmosenv.2009.12.011.

Qin, Y.M., Tan, H.B., Li, Y.J., Li, Z.J., Schurman, M.I., Liu, L., Wu, C., Chan, C.K., 2018. Chemical characteristics of brown carbon in atmospheric particles at a suburban site near Guangzhou, China. Atmos. Chem. Phys. 18, 16409–16418. https://doi.org/10.5194/acp-18-16409-2018.

Querol, X., Pérez, N., Reche, C., Ealo, M., Ripoll, A., Tur, J., Pandolfi, M., Pey, J., Salvador, P., Moreno, T., Alastuey, A., 2019. African dust and air quality over Spain: Is it only dust that matters? Sci. Total Environ. 686, 737–752. https://doi.org/10.1016/j.scitotenv.2019.05.349.

Saleh, R., 2020. From measurements to models: toward accurate representation of brown carbon in climate calculations. Curr. Pollution Rep. 6, 90–104. https://doi.org/10.1007/s40726-020-001393.

Saleh, R., Hennigan, C.J., McMeeking, G.R., Chuang, W.K., Robinson, E.S., Coe, H., Donahue, N.M., Robinson, A.L., 2013. Absorptivity of brown carbon in fresh and photo-chemically aged biomass-burning emissions. Atmos. Chem. Phys. 13, 7683–7693. https://doi.org/10.5194/acp-13-7683-2013.

Saleh, R., Robinson, E.S., Tkacik, D.S., Ahern, A.T., Liu, S., Aiken, A.C., Sullivan, R.C., Presto, A.A., Dubey, M.K., Yokelson, R.J., Donahue, N.M., Robinson, A.L., 2014. Brownness of organics in aerosols from biomass burning linked to their black carbon content. Nat. Geosci. 7, 647–650. https://doi.org/10.1038/ngeo2220.

Saleh, R., Cheng, Z., Atwi, K., 2018. The brown-black continuum of light-absorbing combustion aerosols. Environ. Sci. Tech. Lett. 5, 508–513. https://doi.org/10.1021/acs.estlett.8b00305.

Samek, L., Stegowski, Z., Styszko, K., Furman, L., Zimnoch, M., Skiba, A., Kistler, M., Kasper-Giebl, A., Rozanski, K., Konduracka, E., 2019. Seasonal variations of chemical composition of PM2.5 fraction in the urban area of Krakow, Poland: PMF source attribution. Air Qual. Atmos. Health 13, 89–96. https://doi.org/10.1007/s11869-019-00773-x.

Samset, B.H., Myhre, G., Herber, A., Kondo, Y., Li, S.-M., Moteki, N., Koike, M., Oshima, N., Schwarz, J.P., Balkanski, Y., Bauer, S.E., Bellouin, N., Berntsen, T.K., Bian, H., Chin, M., Diehl, T., Easter, R.C., Ghan, S.J., Iversen, T., Kirkevåg, A., 2014. Modelled black carbon radiative forcing and atmospheric lifetime in AeroCom Phase II constrained by aircraft observations. Atmos. Chem. Phys. 14, 12465–12477. https://doi.org/10.5194/acp-14-12465-2014.

Samset, B.H., Stjern, C.W., Andrews, E., Kahn, R.A., Myhre, G., Schulz, M., Schuster, G.L., 2018. Aerosol absorption: progress towards global and regional constraints. Current Climate Change Reports 4, 65–83. https://doi.org/10.1007/s40641-018-0091-4.

Sand, M., Samset, B.H., Myhre, G., Gliß, J., Bauer, S.E., Bian, H., Chin, M., Checa-Garcia, R., Ginoux, P., Kipling, Z., Kirkevåg, A., Kokkola, H., Le Sager, P., Lund, M.T., Matsui, H., van Noije, T., Olivié, D.J.L., Remy, S., Schulz, M., Stier, P., 2021. Aerosol absorption in global models from AeroCom phase III. Atmos. Chem. Phys. 21, 15929–15947. https://doi.org/10.5194/acp-21-15929-2021.

Savadkoohi, M., Pandolfi, M., Reche, C., Niemi, J.V., Mooibroek, D., Titos, G., Green, D. C., Tremper, A.H., Hueglin, C., Liakakou, E., Mihalopoulos, N., Stavroulas, I., Artiñano, B., Coz, E., Alados-Arboledas, L., Beddows, D., Riffault, V., De Brito, J.F., Bastian, S., Baudic, A., 2023. The variability of mass concentrations and source apportionment analysis of equivalent black carbon across urban Europe. Environ. Int. 178, 108081. https://doi.org/10.1016/j.envint.2023.108081.

Schwarzer, G., Carpenter, J.R., Rücker, G., 2015. Meta-Analysis with R, Use R! Springer International Publishing, Cham. https://doi.org/10.1007/978-3-319-21416-0.

Segersson, D., Eneroth, K., Gidhagen, L., Johansson, C., Omstedt, G., Nylén, A.E., Forsberg, B., 2017. Health impact of PM_{10}, $PM_{2.5}$ and black carbon exposure due to different source sectors in Stockholm, Gothenburg and Umea, Sweden. Int. J. Environ. Res. Public Health 14, 742. https://doi.org/10.3390/ijerph14070742.

Sirois, A.: A brief and biased overview of time-series analysis of how to find that evasive trend, Annex E, WMO/EMEP Workshop on Advanced Statistical Methods and their Application to Air Quality Data Sets, Helsinki, 14–18 September 1998, Global Atmosphere Watch No. 133, WMO TD – No. 956, World Meteorological Organization, Geneva, Switzerland, 1998.

Srinivas, B., Sarin, M.M., 2013. Light absorbing organic aerosols (brown carbon) over the tropical Indian Ocean: impact of biomass burning emissions. Environ. Res. Lett. 8, 044042. https://doi.org/10.1088/1748-9326/8/4/044042.

Su, T., Li, Z., Kahn, R., 2018. Relationships between the planetary boundary layer height and surface pollutants derived from lidar observations over China: regional pattern and influencing factors. Atmos. Chem. Phys. 18, 15921–15935. https://doi.org/10.5194/acp-18-15921-2018.

Sumlin, B.J., Heinson, Y.W., Shetty, N., Pandey, A., Pattison, R.S., Baker, S., Hao, W.M., Chakrabarty, R.K., 2018. UV–Vis–IR spectral complex refractive indices and optical properties of brown carbon aerosol from biomass burning. J. Quant. Spectrosc. Radiat. Transf. 206, 392–398. https://doi.org/10.1016/j.jqsrt.2017.12.009.

Sun, J., Hermann, M., Yuan, Y., Birmili, W., Collaud Coen, M., Weinhold, K., Madueño, L., Poulain, L., Tuch, T., Ries, L., Sohmer, R., Couret, C., Frank, G., Brem, B.T., Gysel-Beer, M., Ma, N., Wiedensohler, A., 2021. Long-term trends of black carbon and particle number concentration in the lower free troposphere in Central Europe. Environ. Sci. Eur. 33. https://doi.org/10.1186/s12302-021-00488-w.

Tian, J., Wang, Q., Ma, Y., Wang, J., Han, Y., Cao, J., 2023. Impacts of biomass burning and photochemical processing on the light absorption of brown carbon in the southeastern Tibetan Plateau. Atmos. Chem. Phys. 23, 1879–1892. https://doi.org/10.5194/acp-23-1879-2023.

Titos, G., del Águila, A., Cazorla, A., Lyamani, H., Casquero-Vera, J.A., Colombi, C., Cuccia, E., Gianelle, V., Močnik, G., Alastuey, A., Olmo, F., Alados-Arboledas, L., 2017. Spatial and temporal variability of carbonaceous aerosols: Assessing the impact of biomass burning in the urban environment. Sci. Total Environ. 578, 613–625. https://doi.org/10.1016/j.scitotenv.2016.11.007.

Tobler, A.K., Skiba, A., Canonaco, F., Močnik, G., Rai, P., Chen, G., Bartyzel, J., Zimnoch, M., Styszko, K., Nęcki, J., Furger, M., Różański, K., Baltensperger, U., Slowik, J.G., Prevot, A.S.H., 2021. Characterization of non-refractory (NR) PM_1 and source apportionment of organic aerosol in Kraków, Poland. Atmos. Chem. Phys. 21, 14893–14906. https://doi.org/10.5194/acp-21-14893-2021.

Updyke, K.M., Nguyen, T.B., Nizkorodov, S.A., 2012. Formation of brown carbon via reactions of ammonia with secondary organic aerosols from biogenic and anthropogenic precursors. Atmos. Environ. 63, 22–31. https://doi.org/10.1016/j.atmosenv.2012.09.012.

Utry, N., Ajtai, T., Filep, Á., Pintér, M., Török, Z.s., Bozóki, Z., Szabó, G., 2014. Correlations between absorption Angström exponent (AAE) of wintertime ambient urban aerosol and its physical and chemical properties. Atmos. Environ. 91, 52–59. https://doi.org/10.1016/j.atmosenv.2014.03.047.

Velazquez-Garcia, A., Crumeyrolle, S., de Brito, J.F., Tison, E., Bourrianne, E., Chiapello, I., Riffault, V., 2023. Deriving composition-dependent aerosol absorption, scattering and extinction mass efficiencies from multi-annual high time resolution observations in Northern France. Atmos. Environ. 298, 119613. https://doi.org/10.1016/j.atmosenv.2023.119613.

Velazquez-Garcia, A., de Brito, J.F., Crumeyrolle, S., Chiapello, I., Riffault, V., 2024. Assessment of light-absorbing carbonaceous aerosol origins and properties at the ATOLL site in Northern France. doi: 10.5194/ar-2024-5.

Viana, M., Alastuey, A., Querol, X., Guerreiro, C., Vogt, M., Colette, A., Collet, S., Albinet, A., Fraboulet, I., Lacome, J.-M., Tognet, F., De Leeuw, F., 2016. Contribution of residential combustion to ambient air pollution and greenhouse gas emissions, European Topic Centre on Air Pollution and Climate Change Mitigation, ETC/ACM Technical Paper 2015/1, https://www.eionet.europa.eu/etcs/all-etc-reports (last access: 23 January 2024), 2015.

Vidgen, B., Yasseri, T., 2016. P-Values: Misunderstood and Misused. Front. Phys. 4. https://doi.org/10.3389/fphy.2016.00006.

Virkkula, A., 2021. Modeled source apportionment of black carbon particles coated with a light-scattering shell. Atmos. Meas. Tech. 14, 3707–3719. https://doi.org/10.5194/amt-14-3707-2021.

Virkkula, A., Mäkelä, T., Hillamo, R., Yli-Tuomi, T., Hirsikko, A., Hämeri, K., Koponen, I. K., 2007. A simple procedure for correcting loading effects of aethalometer data. J. Air Waste Manage. 57, 1214–1222. https://doi.org/10.3155/1047-3289.57.10.1214.

Wang, X., Heald, C.L., Sedlacek, A.J., de Sá, S.S., Martin, S.T., Alexander, M.L., Watson, T.B., Aiken, A.C., Springston, S.R., Artaxo, P., 2016. Deriving brown carbon from multiwavelength absorption measurements: method and application to AERONET and Aethalometer observations. Atmos. Chem. Phys. 16, 12733–12752. https://doi.org/10.5194/acp-16-12733-2016.

Wang, L., Li, Z., Tian, Q., Ma, Y., Zhang, F., Zhang, Y., Li, D., Li, K., Li, L., 2013. Estimate of aerosol absorbing components of black carbon, brown carbon, and dust from ground-based remote sensing data of sun-sky radiometers. J. Geophys. Res.-Atmos. 118, 6534–6543. https://doi.org/10.1002/jgrd.50356.

Wang, J., Liu, D., Ge, X., Wu, Y., Shen, F., Chen, M., Zhao, J., Xie, C., Wang, Q., Xu, W., Zhang, J., Hu, J., Allan, J., Joshi, R., Fu, P., Coe, H., Sun, Y., 2019. Characterization of black carbon-containing fine particles in Beijing during wintertime. Atmos. Chem. Phys. 19, 447–458. https://doi.org/10.5194/acp-19-447-2019.

Washenfelder, R.A., Attwood, A.R., Brock, C.A., Guo, H., Xu, L., Weber, R.J., Ng, N.L., Allen, H.M., Ayres, B.R., Baumann, K., Cohen, R.C., Draper, D.C., Duffey, K.C.,

Edgerton, E., Fry, J.L., Hu, W.W., Jimenez, J.L., Palm, B.B., Romer, P., Stone, E.A., Wooldridge, P.J., Brown, S.S., 2015. Biomass burning dominates brown carbon absorption in the rural southeastern United States. Geophys. Res. Lett. 42, 653–664. https://doi.org/10.1002/2014GL062444.

Weingartner, E., Saathoff, H., Schnaiter, M., Streit, N., Bitnar, B., Baltensperger, U., 2003. Absorption of light by soot particles: Determination of the absorption coefficient by means of aethalometers. J. Aerosol Sci. 34, 1445–1463. https://doi.org/10.1016/S0021-8502(03)00359-8.

WMO/GAW, 2016. WMO/GAW Aerosol Measurement Procedures, Guidelines and Recommendations. Report No.227, https://library.wmo.int/ (accessed 10.09.24).

Wong, J.P.S., Nenes, A., Weber, R.J., 2017. Changes in light absorptivity of molecular weight separated brown carbon due to photolytic aging. Environ Sci Technol. 51, 8414–8421. https://doi.org/10.1021/acs.est.7b01739.

Wu, L., Wu, C., Deng, T., Wu, D., Li, M., Li, Y.J., Zhou, Z., 2024. Field comparison of dual- and single-spot Aethalometers: equivalent black carbon, light absorption, Ångström exponent and secondary brown carbon estimations. Atmos. Meas. Tech. 17, 2917–2936. https://doi.org/10.5194/amt-17-2917-2024.

Yan, J., Wang, X., Gong, P., Wang, C., Cong, Z., 2018. Review of brown carbon aerosols: recent progress and perspectives. Sci. Total Environ. 634, 1475–1485. https://doi.org/10.1016/j.scitotenv.2018.04.083.

Yan, C., Zheng, M., Bosch, C., Andersson, A., Desyaterik, Y., Sullivan, A.P., Collett, J.L., Zhao, B., Wang, S., He, K., Gustafsson, Ö., 2017. Important fossil source contribution to brown carbon in Beijing during winter. Sci. Rep. 7. https://doi.org/10.1038/srep43182.

Yang, F., Zhang, F., Liu, Z., Chen, Y., Zhang, Y., Wu, C., Lei, Y., Liu, S., Xiao, B., Wan, X., Chen, Y., Han, Y., Cui, M., Huang, C., Wang, G., 2024. Emission and optical characteristics of brown carbon in size-segregated particles from three types of Chinese ships. J. Environ. Sci./J. Environ. Sci. 142, 248–258. https://doi.org/10.1016/j.jes.2023.05.045.

Yttri, K.E., Canonaco, F., Eckhardt, S., Evangeliou, N., Fiebig, M., Gundersen, H., Hjellbrekke, A.-G., Lund Myhre, C., Platt, S.M., Prévôt, A.S.H., Simpson, D., Solberg, S., Surratt, J., Tørseth, K., Uggerud, H., Vadset, M., Wan, X., Aas, W., 2021. Trends, composition, and sources of carbonaceous aerosol at the Birkenes Observatory, northern Europe, 2001–2018. Atmos. Chem. Phys. 21, 7149–7170. https://doi.org/10.5194/acp-21-7149-2021.

Yuan, C., Zheng, J., Ma, Y., Jiang, Y., Li, Y., Wang, Z., 2020. Significant restructuring and light absorption enhancement of black carbon particles by ammonium nitrate coating. Environ. Pollut. 262, 114172. https://doi.org/10.1016/j.envpol.2020.114172.

Yus-Díez, J., Bernardoni, V., Močnik, G., Alastuey, A., Ciniglia, D., Ivančič, M., Querol, X., Perez, N., Reche, C., Rigler, M., Vecchi, R., Valentini, S., Pandolfi, M., 2021. Determination of the multiple-scattering correction factor and its cross-sensitivity to scattering and wavelength dependence for different AE33 Aethalometer filter tapes: A multi-instrumental approach. Meas. Tech. Discuss Atmos. https://doi.org/10.5194/amt-2021-46.

Yus-Díez, J., Via, M., Alastuey, A., Karanasiou, A., Minguillón, M.C., Perez, N., Querol, X., Reche, C., Ivančič, M., Rigler, M., Pandolfi, M., 2022. Absorption enhancement of black carbon particles in a Mediterranean city and countryside: effect of particulate matter chemistry, ageing and trend analysis. Atmos. Chem. Phys. 22, 8439–8456. https://doi.org/10.5194/acp-22-8439-2022.

Zalzal, J., Liu, Y., Smargiassi, A., Hatzopoulou, M., 2024. Improving residential wood burning emission inventories with the integration of readily available data sources. Sci. Total Environ. 946, 174226. https://doi.org/10.1016/j.scitotenv.2024.174226.

Zauli-Sajani, S., Thunis, P., Pisoni, E., Bessagnet, B., Monforti-Ferrario, F., De Meij, A., Pekar, F., Vignati, E., 2024. Reducing biomass burning is key to decrease PM2.5 exposure in European cities. Sci. Rep. 14, 10210. https://doi.org/10.1038/s41598-024-60946-2.

Zeng, D., Lin, D.Y., 2015. On random-effects meta-analysis. Biometrika 102, 281–294. https://doi.org/10.1093/biomet/asv011.

Zhang, Y., Albinet, A., Petit, J.-E., Jacob, V., Chevrier, F., Gille, G., Pontet, S., Chrétien, E., Dominik-Sègue, M., Levigoureux, G., Mocnik, G., Gros, V., Jaffrezo, J.-L., Favez, O., 2020. Substantial brown carbon emissions from wintertime residential wood burning over France. Sci. Total Environ. 743. https://doi.org/10.1016/j.scitotenv.2020.140752.

Zhang, Q., Quan, J., Tie, X., Li, X., Liu, Q., Gao, Y., Zhao, D., 2015. Effects of meteorology and secondary particle formation on visibility during heavy haze events in Beijing, China. Sci. Total Environ. 502, 578–584. https://doi.org/10.1016/j.scitotenv.2014.09.079.

Zotter, P., Herich, H., Gysel, M., El-Haddad, I., Zhang, Y., Mocnik, G., Hüglin, C., Baltensperger, U., Szidat, S., Prévot, A.S.H., 2017. Evaluation of the absorption Ångstrom exponents for traffic and wood burning in the Aethalometer-based source apportionment using radiocarbon measurements of ambient aerosol. Atmos. Chem. Phys. 17, 4229–4249. https://doi.org/10.5194/acp-17-4229-2017.